IS-T-405

SUPERCONDUCTIVITY AND MAGNETIC ORDER IN La-Ce ALLOYS

Ph. D Thesis Submitted to Iowa State University, August 1970

John Jerome Wollan

Ames Laboratory, USAEC
Iowa State University
Ames, Iowa 50010

PREPARED FOR THE U. S. ATOMIC ENERGY COMMISSION UNDER CONTRACT NO. W-7405-eng-82

Date Transmitted: September 1970

DISCLAIMER

IS-T-405

LEGAL NOTICE

Printed in the United States of America
Available from
Clearinghouse for Federal Scientific and Technical Information
National Bureau of Standards, U.S. Department of Commerce
Springfield, Virginia 22151
Price: Printed Copy $3.00; Microfiche $0.65

SUPERCONDUCTIVITY AND MAGNETIC ORDER IN La-Ce ALLOYS

by

John Jerome Wollan

A Dissertation Submitted to the

Graduate Faculty in Partial Fulfillment of

The Requirements for the Degree of

DOCTOR OF PHILOSOPHY

Major Subject: Physics

Approved:

D K Finnemore
In Charge of Major Work

D J Mahano
Head of Major Department

K. J. Drey
Dean of Graduate College

Iowa State University
Of Science and Technology
Ames, Iowa

AUGUST 1970

SUPERCONDUCTIVITY AND MAGNETIC ORDER IN La-Ce ALLOYS*

John Jerome Wollan

ABSTRACT

Superconductivity and magnetic order have been studied both above and below the Kondo temperature for the La-Ce system. Electrical resistivity measurements on La 0.2, 1.0, 2.0, 3.2, and 4.0 wt. % Ce have been made from 0.06 K to 20 K. All samples showed a Kondo-like minimum, T_{min}, in the resistivity with a subsequent maximum, T_{max}. T_{min} was found to be proportional to $n^{1/7}$, where n is the concentration, and T_{max} (H = 0) was proportional to n^2. The slope of the resistivity due to the magnetic impurities went as $\rho_\alpha \ln T$ on both sides of T_{max}. Above T_{max} the proportionality constant, ρ_α, was almost independent of n, and below T_{max} it was proportional to n^2. Applied magnetic fields had little effect on ρ_α even though T_{max} increased linearly with H. The magnitude of the resistivity at the peak was essentially independent of n but decreased for increased H. The superconducting transition temperature was depressed as n increased, but more slowly than predicted by Abrikosov and Gor'kov, and the critical field curves were considerably depressed below the multiple pair breaking theory of Fulde and Maki.

---

*USAEC Report IS-T-405. This work was performed under contract W-7405-eng-82 with the Atomic Energy Commission.

TABLE OF CONTENTS

INTRODUCTION

Magnetic impurity states in both normal and superconducting metals have been the subject of extensive theoretical and experimental study. Interest in this problem originally centered around the resistance minimum, giant thermoelectric power, and related phenomena, which occurred when 3d transition metal impurities were dissolved in noble metal matrixes. Somewhat later, investigations on these phenomena were extended through the years to include the 4f impurities as well. Review articles about the problem abound (1,2,3,4). More recently there has been much interest in these magnetic states in superconductors, but for this case there are as yet no satisfactory reviews.

Briefly stated, the problem is this. If an impurity ion which is normally magnetic (e.g. Fe or Gd) is placed in a normal metal host, the host responds and spin correlations develop between the host conduction electron spins and the impurity spins. In the region around the impurity there may be charging effects, hybridization or mixing of the impurity levels with the conduction levels, resonant scattering, or any number of other phenomena taking place. The occurrence of these phenomena is dependent upon the impurity atom retaining its magnetic moment. Originally attempts were made to view the response of the host within the independent particle picture, but it now seems clear that many body effects are crucial for a complete understanding (3).

The most obvious and easily observed manifestation of these spin-spin correlations is a minimum in the low temperature resistivity, ρ. This was first seen in some presumably pure metals by Meissner and Voigt (5) in 1930.

Later work by de Haas, de Boer and van den Berg (6) on various purities of Au also exhibited a similar minimum. Resistance measurements on dilute alloys of manganese in silver by Gerritsen and Linde (7) in 1949 were the first systematic study of this phenomena. The extensive investigation of 3d impurities in noble metals showed that minima existed, for example, when Fe (8), Cr (9), or Co (9) were dissolved in Cu. For Cr in Au (10) and for Mn in Au (10), Cu (10) or Ag (11) a lower temperature maximum was found as well as a minimum.

Systematic studies by Sugawara (12) and Sugawara and Eguchi (13,14) of rare earth solutes in both Y and La have shown that Ce is the only rare earth impurity to show a resistance minimum. In a similar study by Peterson, Page, Rump and Finnemore (15) with Th as the host material no resistance minima were found whatsoever. Consequently Kondo type investigations involving rare earths have reduced to the study of Ce impurities.

A complicating feature of all these investigations is that some host-impurity combinations form a local moment and others do not. For example, Mn in Cu (10) seems to form a moment but Mn in Al (16) does not. Or to complicate matters further, in Mo-Nb alloys Fe impurity ions change from being nonmagnetic to magnetic when the concentration is varied only a few percent. The formation of such moments must be a very delicate balance.

Anderson (17) provided the first clue to understanding the formation of these moments in 1961. In that paper he showed that mixing or hybridization of an impurity level with the conduction electron states in the metal drove both spin up and spin down impurity levels toward the Fermi

level. Hence this mixing tended to drive the impurity toward a non-magnetic state in which both spin states were equally occupied. This is a cooperative, many body effect, and consequently the transition from magnetic to non-magnetic states is quite precipitate. Within this model the magnetic or non-magnetic character of an impurity state depends upon the relative strengths of the Coulomb energy and the hybridization term.

Kondo (18) gave the first theoretical explanation of the resistance minimum (hence the name Kondo effect) by a second Born approximation calculation of the excess scattering of the conduction electrons due to the magnetic impurities. He found the excess resistivity to be proportional to $nJ^3 \ln(T/D)$, where n is the impurity concentration, J is the exchange integral for the s and d electrons, and D is the bandwidth. Consequently for J negative, ie. antiferromagnetic coupling, there will be a logarithmic singularity as T goes to zero. A true singularity will always be troublesome, but the model at least showed how the minimum might arise, and it provided a guide for the temperature dependence.

Since these original calculations Kondo (19), Yosida (20), Nagaoka (21) and others (3) have extended this s-d exchange model and have shown that the apparent singularity at T = 0 does not occur because a "spin compensated state" is formed. This was described as a quasibound state in which the conduction electrons formed an antiparallel "cloud" around the magnetic impurity spin, hence reducing its effective moment to zero. The lnT singularity then goes smoothly to a ρ = constant behavior as T goes to zero.

Further work by Abrikosov (22), Suhl (23) and Kondo (24) (denoted as

ASK) has shown that a resonant scattering model can produce a minimum in ρ and a subsequent maximum at a temperature, T_{max}, related to J and the Fermi energy ϵ_F. In addition the theory predicts that T_{max} is independent of the impurity concentration, and that the additional resistivity is approximately proportional to $nJ^3 \ln T$ below as well as above T_{max} and tends to zero as T tends to zero. This theoretical work, however, assumes very dilute concentrations so some modification will be required before it is applied to concentrations of several percent.

The most recent theoretical work has centered around the localized spin fluctuation (lsf) model of Suhl (25) and Levine et al. (26) in which local spin fluctuations out of an Anderson-like ground state result from repeated conduction electron-hole scattering at the impurity site. When the relaxation time for these fluctuations is shorter than the relaxation time for other relevant electronic processes (e.g. 10^{-12} seconds for superconducting Cooper pairs), then the alloy is nonmagnetic. For this theory the low temperature resistivity is predicted to follow a $\rho_o(1-T^2/T_o^2)$ behavior.

Unfortunately details of the local spin interactions with the conduction electrons are not known, and hence one cannot predict which of these theories is more likely to apply for a given alloy system. If, however, one of these seems to describe the normal state properties of an alloy system, then one might infer some of the details of the magnetic impurity state and the interactions involved. Figure 1 shows the basic form of the low temperature resistivity for the various theories.

If the host material for the magnetic impurities undergoes a

superconducting transition, the problem seems to become even more complicated. In addition to the impurity spin correlations associated with the normal state, a superconductor has spin correlations associated with the formation of Cooper pairs (27). In a sense the problem can be viewed as a competition between these two kinds of spin correlations.

In 1961 Abrikosov and Gor'kov (28) (AG) presented a theory for the case of non-interacting, paramagnetic impurities in a superconductor. In this theory all the properties of the magnetic impurity were described with one parameter, the life-time broadening (Γ) of the Cooper pairs due to spin scattering. The theory predicted three major results. First, a lowering of the superconducting transition temperature (T_c) as the impurity concentration (n) is increased, until $T_c = 0$ at some critical concentration n_{cr}. Second, a lowering of the critical field curves below the BCS (27) values. Third, the disappearance of the gap in the single particle density of states for n greater than $0.9\ n_{cr}$. Experimental verification for this theory is well established. One of the first of these was a series of tunneling experiments by Reif and Woolf (29) on In-Fe and Pd-Gd which showed the disappearance of the gap, but there were more states in the gap than the theory predicted. Millstein and Tinkham (30) did very precise tunneling measurements on Sn and Sn-In alloys and also got good agreement with theory. The critical field curve measurements on Th and Th-Gd alloys by Decker and Finnemore (31) gave agreement with the theory in the paramagnetic region. In addition, Maple's results (32) for T_c of $La_{1-x}Al_2Gd_x$ out to $n = 0.9n_{cr}$ followed the T_c vs. n curve predicted by AG. Although AG theory has been well established in the paramagnetic region, further

extension of the theory is necessary if ordering occurs or if Γ is a function of temperature.

Major deviations from the AG T_c versus n curve were first noted by Matthias et al. (33) and Hein et al. (34) in the La-Gd system. At high concentrations they found that the T_c versus n curve had a hump well above the AG prediction. Crow and Parks (35) also found deviations from AG theory at n close to n_{cr} in the In $La_{3-x}Gd_x$ system and attributed them to impurity coupling effects.

Bennemann (36) gave a more complete theoretical explanation for these data, based on magnetic ordering of the impurities. It involved the interplay of three different effects--first, the reduction in spin flip scattering; second, the gliding of the Fermi surface due to the average exchange field; and third, the spin-orbit scattering which tends to moderate the second effect because the normal state wave function spin states are mixed. With a combination of these effects he was able to explain most of the features of the T_c versus n curves for In $La_{3-x}Gd_x$ and La-Gd.

Corrections to the AG critical field curves have been given by Fulde and Maki (37) and by Bennemann, Garland and Mueller (38). Fulde and Maki extended the theory to type II superconductors by considering the added pair breaking effect caused by the penetration of the magnetic field, H, in the intermediate state. This is known as the multiple pair breaking theory since, in addition to the breaking up of Cooper pairs by impurity spin flip scattering, the penetrating magnetic field removes allowed Cooper pair states by shifting the spin up Fermi surface relative to the

spin down. The extension of the ideas of Fulde and Maki by Bennemann et al. (38) known as the exchange field enhancement effect, is also a result of the penetrating external field. Within Bennemann's model, the external field orients some of the impurity ions, and the impurity ions in turn orient some of the conduction electrons because they are coupled to them via the exchange field. This mechanism can then enhance the ability of the applied field to change the conduction electron spin population and hence destroy superconductivity. Critical field curves of La-Lu and La-Lu-Th alloys measured by Williams, Decker and Finnemore (39) showed good agreement with the multiple pair breaking scheme for La-Lu. With 0.85 % and 1.0 % Tb, however, the critical fields at T = 0 were only about 50 % of the value predicted by multi-pair breaking theory. The difference was attributed to the exchange field enhancement effect.

The localized spin fluctuation (lsf) model has been applied to the case of superconducting hosts by Bennemann (40). For this situation the lifetime of a localized spin fluctuation varies inversely as the temperature, and this in turn makes the Cooper pair lifetime increase as the temperature is lowered. Hence, Tc will not be depressed as rapidly as predicted by AG where Γ was independent of temperature. Early qualitative agreement with this theory has been shown by Maple et al. (41) for Th-U alloys.

Cerium, as has been pointed out, has the unique distinction of being the only rare earth impurity to exhibit a resistance minimum. As a result there has been considerable investigation of its alloys and in particular the La-Ce system. Despite this fact no work has been done for $T \ll T_k$,

which is the region of great interest from a theoretical point of view. Consequently a series of measurements on the resistivity, magnetoresistance, superconducting transition temperature, and critical fields of dilute Ce in La was undertaken. The fact that La and Ce have the same valance (+3), approximately the same size and atomic weight, and are mutually soluble makesthis a metallurgically ideal system. The one main problem is the existence of two crystal structures of the La host, fcc and d-hcp, which sometimes complicates the interpretation of the superconducting results.

EXPERIMENTAL CONSIDERATIONS

Equipment

A He^3-He^4 dilution cryostat was used for all measurements done in this experiment. The principles of operation of these devices have been well described in a number of review articles (42,43,44), so only a brief summary of the theory will be given here. A more detailed description of the construction and operation of the cryostat will be given, however, because these details govern the accuracy of the measurement.

Two essential ingredients for the operation of He^3-He^4 cryostat are the positive entropy of mixing of He^3 and He^4, and the phase separation of He^3 and He^4 mixtures at low temperatures. Below .8 K a He^3-He^4 mixture phase separates into a He^3 rich phase floating on top of a superfluid He^4 rich phase. As the temperature decreases, the He^3 rich phase becomes essentially pure He^3 with practically no solubility of He^4 in the He^3. The He^4 rich phase, however, approaches a solution of 6 % He^3 in He^4. If some of the He^3 which is dissolved in the He^4 rich phase were removed (by pumping for example), then osmotic pressure would drive He^3 across the phase boundary to maintain equilibrium. The adiabatic mixing then produces the cooling. To obtain a continuously operating refrigerator, one must then separate the He^3 from the He^4 by a distillation process and return the separated He^3 to the mixing chamber.

Details of the apparatus are shown in Figure 2. The phase boundary between the He^3 rich phase and the He^4 rich phase occurs in the mixing chamber. This is the source of refrigeration, and hence the sample holder is attached here. In normal operation He^3 expands across the phase

boundary and flows through the He^4 up the dilute side of the heat exchangers to the still. Here the He^3 and He^4 are separated by fractional distillation (hence the name "still"). A half milliwatt of heat is required for efficient operation of the still. Ideally a temperature of 0.6 K to 0.7 K is maintained at the still so that little He^4 is pumped away despite the fact that the concentration in the still is about 99 % He^4. Any He^4 which is circulated has to be phase separated when it returns to the mixing chamber, so it is a source of heat load on the system. Under normal conditions the ratio of He^3-He^4 circulated is about 8/1. The He^3 which has been distilled returns to a heat exchanger or condenser located on the He^4 chamber where its heat of vaporization is removed. A flow impedance between the condenser and the still heat exchanger assures that the pressure of the returning gas of the condenser will be high enough to cause liquefaction. The still heat exchanger and a similar flow impedance below it provide a further guarantee that all the gas is liquified. In addition, this heat exchanger cools the returning He^3 from 1 K to 0.6 K. The He^3 then flows down the concentrated side of the four heat exchangers and is cooled by the rising He^3 in the dilute side. The cooling cycle is completed when the returning He^3 enters the top of the mixing chamber. The whole system is enclosed in a vacuum can which is maintained at 4.2 K.

The external gas handling system is shown in Figure 3. A special valving system allows a Veeco MS 9AB leak detector, which has been modified to detect He^3 as well as He^4 (45), to monitor the He^3/He^4 ratio of the gas being pumped. An NRC-B4 booster diffusion pump backed by a sealed shaft Welch-1402KGB mechanical pump was used to pump on the still. The gas lines from the mechanical pump and the storage tanks pass through high

density concrete blocks to reduce vibrations coming into the cryostat. The frame supporting the cryostat and all the plumbing is mounted in sand to further reduce vibrations.

The mechanical pump was a constant source of air and oil leaks into the system, consequently a 77 K trap and a 4.2 K trap were installed to prevent these impurities from reaching the fine capillary tubing in the cryostat itself and plugging the system. Even with these precautions plugging was still a constant problem.

Thermal contact, both liquid to metal and metal to metal is one of the difficult problems involved in working at very low temperatures. To assure adequate heat exchange between the liquid He^3 and He^4 and the metal containers, the heat exchangers and mixing chamber were made with sintered copper plugs. This greatly increased the surface area for heat exchange and thus enhanced thermal contact. Oxidation of this sintered copper during soldering operations which would impede heat exchange may have been a mistake in the construction of the cryostat. Another problem in construction of these sintered plugs was to get the sintered copper to stick to the walls of the cylinder. This problem was finally solved by cutting down the wall thickness of the cylinder to about 0.5 mm and by scoring the inside surface with a lathe tool. The cylinders were then packed with 99.9 % pure 325 mesh copper powder at 2600 lbs/sq in. and sintered for one hour at 800° C in a charcoal reducing atmosphere.

One set of cylinder caps for the concentrated and dilute side of the heat exchangers was silver soldered together to provide heat exchange between the two cylinders. The interconnecting stainless steel capillary

tubing (#19 gauge on the dilute side and #24 gauge on the concentrated side) was silver soldered to the caps which, in turn, were soldered onto the cylinders with Wood's metal. A series of hollow graphite turnbuckles provide the main support for the whole system and thermal isolation between the various components. The flow impedances were made by feeding a 10(-) mil stainless steel wire into the 10 mil I.D. stainless steel capillary.

Because leaks continually developed in the Wood's metal joints, the heat exchangers and mixing chamber were rebuilt. The stainless steel tubing was replaced by 39 mil I.D. 70-30 cupro-nickel tubing, and the Wood's metal joints were redone with regular 50-50 soft solder.

The still temperature in this cryostat was about 1 K which is considerably warmer than it should have been. This may have happened because the still heater was placed outside the still rather than being immersed in the liquid. This did not seem to adversely affect the He^3/He^4 ratio (which was about 8/1) or the heat input necessary to maintain the proper circulation rate of He^3.

A 1.0 K heat shield was mounted on the still to reduce radiation heating to the heat exchangers and mixing chamber. The "coil-foil" heat shield was constructed by winding #40 insulated copper wires on 5 mil mylar and gluing it down with GE 7031 insulating varnish. The mylar and wire combination was then taped around a form with regular Scotch tape to give it the proper shape. The top half inch of mylar was cut off, and the copper wire foil was clamped to the still with Apiezon N grease providing thermal contact. Three graphite spacers were glued to the heat shield to

center it in the vacuum can.

Data between 4.2 and 20 K were taken by applying heat to both the mixing chamber and still. (Heaters consisted of about 1500 Ω of .9 mil Pt - 8% W wire.) Between about .7 and 4.2 K the temperature was maintained by pumping the He^4 pot to 1 K, circulating about 10% of the gas charge of the dilution system, and applying the proper amount of heat to the mixing chamber. Data below .7 K was taken while running the dilution cryostat at full capacity and adding the necessary heat to the mixing chamber (see Table 1).

Table 1. Approximate cooling power of He^3-He^4 cryostat with a still power of .5 mW, still temperature of 1.0 K and condensation pressure of about 40 mm of Hg.

$\dot{Q}_{mc}$, (erg/sec)	T_{mc}, (K)
3	.060
20	.070
40	.080
60	.090
90	.100
130	.110
200	.150

Thermometry

Since temperatures in which data were taken varied over such a wide range, no single thermometer could be used. For data taken between 0.3 K and 20 K, a previously calibrated germanium resistor, GR 251, was used as

the thermometer. This resistor had been calibrated with a constant volume gas thermometer from 4 K to 20 K, with He^4 vapor pressure from 1 K to 4 K and a paramagnetic salt from 0.3 K to 1 K. For data taken between 0.14 K and 0.3 K another previously calibrated germanium resistor, GR 665 was used as the thermometer. It was calibrated with a paramagnetic salt from 0.14 K to 1 K. From 0.3 K to 1 K these two thermometers agreed within $\pm$ 5 mK. Measuring currents varied from 0.2 μa for GR 665 at 0.14 K to 10 μa for GR 251 from 4.2 K to 20 K. There was considerable self heating in GR 251 and in the AC calibration of GR 665 discussed later. Because the measuring configuration was not changed and the calibrations were reproducible, this was not considered a problem. A set of mercury cells furnished a constant current stable to 1 part in 10^5. Voltages were read with a Darcy model 440 digital voltmeter capable of 1 μv resolution.

For temperatures below 0.14 K GR 665 and 2 Speer carbon resistors were calibrated with a cerium magnesium nitrate (CMN) paramagnetic salt. Resistances were measured with a three terminal AC bridge rather than the four terminal DC measurement to keep the power levels below 10^{-9} watts. The AC calibration was actually carried out from 0.060 K to 1.0 K, but the previous DC calibrations were more sensitive at the warmer temperatures.

A 47.4 Hz Whetstone bridge (Figure 4) was used for measuring the resistances. The operating current was nominally 0.1 μa but decreased as much as 10% as the resistance of GR 665 rose to 10^5 Ω at 0.06 K. A General Radio model 1433-F decade resistance was used to balance the bridge, and a dual phase lock-in detector (designed and constructed in the Ames Laboratory electronics shop) was used as a null indicator. A

decade capacitance box across the 5 KΩ standard balanced any stray inductive voltages.

The AC calibration was carried out as follows. Between 0.3 K and 1 K the susceptibility of the cerium magnesium nitrate was measured as a function of temperature using the previous calibration of GR 251. The AC resistance of GR 665 and the two Speer carbon resistors was then measured as a function of the salt susceptibility over the entire temperature range. Because Curie's Law is known to be valid (46) for CMN down to 0.006 K, the temperatures below 0.3 K were determined by extrapolating the high temperature X vs 1/T calibration.

The bridge used in measuring the susceptibility of the salt is shown in Figure 5. The voltage induced in the astatically wound secondary of the susceptibility coils was balanced by picking off the necessary voltage from a mutual inductance lump with a Gertsch model 1011 ratio standard. Null in the secondary circuit was determined by another dual phase lock-in detector. Any stray out of phase voltages were cancelled by applying the necessary voltage across the 1 Ω resistor. The oscillator output was set such that the salt measuring field was 0.5 Oe.

The physical set up for the calibration is shown on the right side of Figure 6. The four resistors were mounted in the resistor block with Apiezon N-grease, and the leads were connected to thermal grounding strips mounted around the block. Nine #20 copper wires, silver soldered to the block, provided thermal contact between the CMN in the nylon cylinder and the thermometers. A heat shield surrounded the whole system. The susceptibility coils were mounted outside the can in place of the

superconducting solenoid shown on the left.

The CMN crystals were grown from a saturated solution of cerous nitrate and magnesium nitrate. The crystals were quickly dried, ground into a fine mush in Dow Corning 200 fluid and packed into the nylon cylinder. The 200 fluid prevented the waters of hydration from evaporating and also gave thermal contact between the wires and the salt.

Sample Preparation

Samples were prepared from ingots of pure La and Ce obtained from B. Beaudry and F. H. Spedding of this laboratory. Impurities in these starting materials are given in parts per million (ppm) in Table 2. Approximately 50 grams of La was cut from the initial ingot and weighed. Then, using 138.91 gm/mole and 140.12 gm/mole for the atomic masses La and Ce respectively, the appropriate amount of Cerium needed for nominally 0.2, 1.0, 2.0, 3.2 and 3.5 at.% Ce (at. % will usually be shortened to %) in La was calculated. The pieces of sample were electropolished in a 5% perchloric acid solution (47) and weighed to the nearest .1 mgm. Table 3 shows the weights used and the exact percent Ce for each alloy. The percent Ce determined by chemical analysis is also included. (This will be discussed later.)

The constituents for a given sample were then placed on a water cooled copper plate in a standard arc-melter. The plate had been cleaned previously with a 50% nitric acid solution. The arc-melter was then evacuated and flushed 5 times with He gas and finally bleed up to about minus 5 inches of Hg. Before arc melting the sample a zirconium getter button

Table 2. Impurities present in the starting materials in ppm by weight (blank spaces indicate no test was run for the material listed). The 1.03, 2.02 and 3.23% samples were made from La_1 and Ce_1, and the .22 and 3.98% samples were made from La_2 and Ce_2

Impurity	La_1	La_2	Ce_1	Ce_2
H	6	25	7	3
C		61		22
N	4	5	3	4
O	111	262	136	63
F				28
Mg	<10	≤10	<40	1.4
Al	20	<10	<60	1.2
Ca	3	<10	9	2
Sc	0.6			1.3
Cr	2	≤10	2	0.7
Mn	0.3		0.2	0.1
Fe	20	4.8	8	3.2
Co	0.08			0.04
Ni	10	≤10	2	4.2
Cu	5	10	2	1.8
Y	1	≤20	100	1.27
Pr	70	<280	70	10
Nd	12	<200	20	51
Gd	20		160	45
Tb	2		20	<7
Dy	1		60	8
Ho	2		20	6
Er	2		20	12
Tm	0.1		0.1	0.1
Yb	0.6		0.6	<1.2
Lu	0.4		0.4	0.25
Ta	7	≤500	80	39
W		≤200		

Table 3. Composition of the alloys.

Nominal percent Ce	Weight in gm(moles) of La	Weight in gm(moles) of Ce	Exact percent Ce by weight	Percent Ce by chemical analysis
0.2	37.5001 (.269960)	.0758 (.000541)	.200	.22 ±.01
1.0	53.7759 (.387128)	.5642 (.004027)	1.0295	1.03 ±.03
2.0	51.3899 (.369951)	1.0744 (.007668)	2.0306	2.02 ±.02
3.2	57.2133 (.411873)	1.9073 (.013612)	3.1992	3.23 ±.01
3.5	37.4954 (.269926)	1.3718 (.009790)	3.5000	3.98 ±.01

was melted at 210 amps to remove any traces of oxygen still in the system. The sample was then melted at 250 amps for about 1 minute, flipped and remelted for a total of ten times except for the 1.0% sample which was only melted 4 times. The samples were then melted into a 1/4 inch diameter by 3 inch long finger. During this process one of the samples (La 1.0% Ce) was fused to the copper plate slightly, and traces of copper

could be seen on the surface. Because the final samples were cut from the center of the finger this should have had no effect on the results.

The 1.0, 2.0 and 3.2% fingers were glued to a brass slab and a sample approximately .3 cm square by 6 cm long was spark cut from the center. The 0.2 and 4.0% Ce samples were cut out on a diamond saw. The samples were then glued to a lapping tool and ground down, using various grades of sandpaper, to the proper size (see Table 4) and polished. The polishing was done with 600 grit paper soaked with Dow Corning 200 fluid.

Table 4. Sample Sizes

Nominal Ce concentration %	height (cm)	width (cm)	length (cm)	$A/\ell \times 10^{+3}$ (cm)
0.2	.1531	.1845	4.96	5.695
1.0	.1314	.1978	6.66	3.902
2.0	.1060	.1531	5.85	2.774
3.0	.1041	.2029	6.54	3.230
4.0	.1318	.1318	5.10	6.295

The samples were then electropolished and sealed in an outgassed tantalum tube which had been flushed three times and filled with He. The tantalum tube was then similarly sealed in a quartz tube and the whole system placed in an annealing furnace at 250°C. Annealing times were 93 hours for the 2.0 and 3.2% samples, 108 for the 1.0% sample and 63 hours for the 0.2 and 4.0% samples.

Lanthanum exists in two different crystal structures, fcc and d-hcp, d-hcp being the stable phase below 300°C. During the fast cooling after the samples were arc melted, a small amount of fcc structure was "quenched in". Neutron diffraction studies of the 2.0 and 3.2% samples before annealing showed about 7% fcc phase present. The short anneal times reduced strains in the samples, but probably had little effect on the amount of fcc phase present.

After the data had been taken, a number of parameters (e.g. Figures 7 and 8) showed a kink between the supposed 3.2 and 3.5% samples. This seemed to indicate that a mistake in weighing might have occurred. Consequently a chemical analysis was performed on all the samples by Mrs. Sandra Gerlock of this laboratory. Table 3 shows the results of this work. (The complete results are given in Appendix A.) Because of the very good agreement with the first four samples it was decided that a mistake in weighing the supposed 3.5% sample had occurred, and hence the value of 3.98% Ce was taken as the correct one.

Measuring Techniques

After the samples were annealed, they were mounted two at a time on the sample holder (Figure 6). The sample holder was an 1/8" thick copper plate 3/4" wide and 9" long. The top was 1/4" thick with holes drilled through for the carbon and germanium resistors. The resistors were wired to manganin grounding strips glued to the sides with GE 7031 and insulated with cigarette paper. The sample holder was also covered with cigarette paper glued on with GE 7031 for electrical insulation. The samples were

clamped onto the holder with 1/16" thick, copper plates which screwed down onto the 1/8" plates and were insulated as above on both sides. Apiezon N-grease was used as a thermal contact agent. The clamping process was used to get the best possible thermal contact between the sample and the holder. A copper disc, which was silver soldered to the top of the sample holder, screwed to the flange on the bottom of the mixing chamber and provided thermal contact to the cryostat. The disc also supported a heat shield.

The magnetic field was produced by a Varian model x - 4122 superconducting solenoid with a rated field of 15 KOe at 22.4 amps. The magnet current was supplied by a Spectromagnetic current regulated power supply. A Keithley model 662 guarded DC differential voltmeter monitored the voltage across a 0.01 Ω Rubicon series resistor to determine the current and hence the field.

Electrical connection for the 0.2, 1.0, and 4.0% samples was made by special knife-edge contacts which were tightly screwed down on to the samples. The contact clamps consisted of a 1/16" by 1/2" by 3/4" copper plate which had a piece of 2 1/2 mil mylar epoxied (Armstrong A-12) on one side. Epoxied on top of the mylar, which provided electrical insulation, were two triangular copper contacts; one current, one potential. Soldered into a hole in each contact was a piece of #18 copper wire which went to a copper, thermal grounding strip mounted on the back of the sample cover plate.

For the 2.0 and 3.2% samples electrical contact was made by ultrasonically soldering #24 copper wires to the samples. The samples were first

tinned with pure indium solder, and the wires were then soldered on with pure tin solder. Tin had to be used since In proved too soft to hold the wire. The wires were then soldered to the grounding strips as before. The switch was made to mechanical contacts because it was felt that any local stress to the sample would be far less detrimental than the heating required for soldering. Also the soldered contacts appeared to have a high resistance. Oxidation of the La surface could have been the cause of this high resistance.

All lead resistances were kept to a minimum because of the need to reduce heating in the cryostat and because of errors in the resistance measurements. In addition, heat leak to the samples via thermal conduction had to be kept to a minimum. Consequently six, 6 mil, lead-coated manganin wires about twenty-four inches long were run from a terminal strip at the top of the vacuum can to the thermal grounding strips on the cover plates (2 current and 4 potential, the samples being wired in series). Below 7 K lead is superconducting so there was no I^2R heating, and the thermal conductivity was lowered so there was negligible heat leak to the samples. Number 32 copper wires ran from the terminal strip at the top of the can through a mylar epoxy feed through to another terminal strip in the bath. Cloth covered #18 manganin leads ran from there to the top of the cryostat where they make connection with the measuring bridge.

The sample resistance was measured by an AC technique instead of the usual DC potentiometric method because of its increased sensitivity, low power input to the samples and speed of measurement. Operating currents

ranged from 4 ma peak to peak at the lowest temperatures to 40 ma at higher temperatures. Sample resistances at 4.2 K ranged from .2 to .9 mΩ so that the heat input from the samples was a maximum of .5 μ watts, which is within the cooling power of the refrigerator at .070 K.

The AC resistance bridge is shown on Figure 9. The voltage set up across the sample was measured by just picking off with the ratio transformer an equal resistance from the standard. A variable mutual inductance balanced out any stray inductive voltages, and a dual phase lock-in detector acted as a null detector. The standard resistor for room temperature measurements was a Leeds and Northrup 4020-B precision 1 Ω resistor. For low temperature measurements two standard resistors were constructed out of 1 inch manganin strips. They were calibrated with the bridge and also potentiometrically against the 1 Ω standard. The bridge values for the standards were 1.1610 mΩ and 4.5888 mΩ which agreed within .2% of the DC values. The resistance of the sample determined which standard was used. At the lowest power levels the bridge sensitivity was about 1% or 4 nanovolts.

Since the sample and standard resistances were so small, voltage losses in lead wires had to be considered. The input impedance of the Gertsch RT 61 at 47 Hz was about .7 MΩ. Since the lead resistance between the standard and the Gertsch was less than 1 mΩ, lead losses were insignificant. The input impedance of the Gertsch ST 248 B in the sample loop was only 20 KΩ at 47 Hz, and the lead resistance was about 2 ohms. Consequently the error due to line losses was measured and found to be less than 2×10^{-4}. The bridge was checked further by measuring the resistance of

a 1/2 inch copper rod at various lengths and comparing it with a DC potentiometric measurement. A 50 ma current was supplied by a constant current source, and the voltages were measured with a Guildline 9180-B potentiometer and a 5214/9460 photocell galvanometer amplifier. For resistances between 0.08 and 0.2 mΩ the difference in the AC and DC measurements ranged from .3 to 1.5% when measured at 40 ma AC. Unfortunately the large copper rod was a good source of pickup which was responsible for the error.

RESULTS AND ANALYSIS

Normal State Properties

Resistivity for the La-Ce alloys studied here all show a Kondo-like minimum similar to the curve for La 4.0 % Ce shown on Figure 10.

Matthiessen's rule (48) has been assumed in separating the various contributions to the resistivity. Hence we write $\rho = \rho_d + \rho_{e\phi} + \rho_l(T) + \rho_m(T)$, where ρ_d is the resistivity due to the accidental "dirt" such as carbon, oxygen, etc., $\rho_{e\phi}$ is the resistivity due to Ce potential scattering, $\rho_l(T)$ is the resistivity due to phonon scattering, and ρ_m is the resistivity due to spin scattering. Above 14 K, where $\rho_m(T)$ is zero, the data are of the form $\rho_o = A + BT^{2.25}$ (Figure 11), where A and B are constants given in Table 5.

Because B is essentially independent of Ce concentration for all

Table 5. A, B, A - ρ_d, (A - ρ_d) / % Ce for the alloys

Sample (wt. % Ce)	A ($\mu\Omega$ - cm)	B $\frac{(\mu\Omega - cm)}{(K)^{2.25}}$	A - ρ_d ($\mu\Omega$ - cm)	(A - ρ_d)/% Ce $\frac{(\mu\Omega - cm)}{\%\ Ce}$
0.22	0.841	3.342×10^{-3}	0.09	0.41
1.02	1.216	3.362	0.47	0.46
2.03	1.732	2.994	0.98	0.47
3.23	2.245	3.168	1.50	0.46
3.98	2.843	3.256	2.09	0.52

samples, and because all samples follow the same exponential form $T^{2.25}$,* we are confident that this term is representative of the phonon scattering. This is a reasonable result since for transition metals one expects a power law between T^2 (49,50,51) and T^3 (52,53) rather than the T^5 (54) law of the noble metals. The T^3 term arises because metals in which s-band carriers scatter into d (or f) - band states require no multiple scattering to relax the electrons as is the case for the T^5 law. In addition to this interband scattering one expects a T^2 result for electron-electron scattering if the electrons have different effective masses.

The constant A varies linearly with Ce content (Figure 8), and we interpret this as a temperature independent scattering term which includes scattering from unwanted impurities as well as cerium potential scattering. The value of ρ_d, found by extrapolating A to n = 0 (Figure 8), is 0.75 $\mu\Omega$ - cm.

The temperature of the resistance minimum, T_{min}, varies with concentration as $n^{1/7}$ (Figure 12). These particular alloys have concentrations which are high enough to expect impurity-impurity coupling, so no obvious physical significance should be given to this fact. For very low concentrations, ~ 100 ppm Ce, the Kondo theory predicts that T_{min} should be proportional to $n^{1/p}$ where p is the exponent of the lattice resistivity term, which in this case is 2.25. Arajs and Anderson (55) found fairly similar results for T_{min} on the same system, but Sugawara and Eguchi (14) found T_{min} to be a function of crystal structure only.

---

*The 1.0, 2.0, and 3.2 % samples could also be fit to $T^{2.5}$, but the more complete data at higher temperatures on the other two samples show that a $T^{2.25}$ fit is the correct one.

Below 14 K the magnetic contribution to the scattering becomes important. This term can then be written $\rho_m(T) = \rho_{total} - \rho_o$, where $\rho_o = A + BT^{2.25}$ from high temperature data. Some qualitative observations can be made.

1) All samples show a sharp rise in ρ_m at 12 K and a ρ_1 lnT dependence between 10 K and 4 K (Figure 13 through 18).

2) All samples exhibit a maximum in ρ_m* with the exception of La 1.0 % Ce which could not be driven completely normal below 2.5 K.

3) The proportionality constant, ρ_1, is not proportional to n as expected from the simple Kondo theory because there are Ce-Ce interactions at these high impurity concentrations. It is also independent of applied field, H.

4) The maximum value of ρ_m is essentially independent of concentration, but dependent upon H.

5) The temperature at which the maximum occurs, T_{max}, is a function of both concentration and applied field.

6) Below T_{max}, as above, ρ_m is proportional to lnT where ρ_2, the proportionality constant, is dependent on concentration but independent of H.

Many of the above observations will require complicated theoretical

---

*The magnitude, but not the shape, of ρ_m is dependent upon the high temperature fit of ρ_o. A $T^{2.5}$ fit instead of a $T^{2.25}$ fit lowers ρ_m but does not change its basic character (Figure 19).

explanations, but at least two points can possibly be understood in terms of fairly simple arguments. The first is that the magnetic field dependence of T_{max} obeys $kT_{max}(H) = \vec{\mu}\cdot\vec{H}$ where μ = 1 Bohr magneton. Hence the peak shifts linearly with Zeeman splitting. Second, the concentration dependence of both T_{max} and ρ_2 goes as n^2 (Figure 20). The probability of finding two cerium atoms an adjacent sites also goes as n^2 so it may be that the strength of the resonant interaction depends on the probability of finding two adjacent Ce atoms.

Cerium seems to have a well defined moment in lanthanum (56) so Kondo's approach (18), therefore, makes a convenient starting place for analyzing the data. Although the data do show a logarithmic divergence below 12 K, the deviations from this behavior below 1 K show that the original Kondo theory no longer applies. Indeed, deviations from the predicted concentration dependence above 1 K indicate it is not applicable there either. The occurence of a maximum in the resistivity is also in disagreement with the Kondo theory as modified by Yosida (20) and Nagaoka (21), and hence it would appear that the local moment is maintained at all temperatures. Consequently it would seem that theoretical approaches similar to those of Abrikosov (22), Suhl (23) and Kondo (24) (ASK) may be most applicable for La-Ce, or the Ce moments may be simply magnetically ordering at low temperatures.

A somewhat more detailed, though still very qualitative, analysis can be made. The temperature independent contribution to the resistivity due to the Ce impurities, $A - \rho_d$ is plotted in Figure 21 as a function of n and has a slope of 1.03. Hence the potential scattering is proportional

to the cerium concentration. The ln T term, however, is not proportional to concentration (Table 6) which implies that the deviation in the concentration dependence of ρ, and also T_{min} may be due to a concentration dependent J. If we assume $\rho_m = \rho_1 \ln T = \alpha n J^3 \ln T$ (3), then $\rho_1 = \alpha n J^3$ where α includes the appropriate constants. Since ρ_1 is only weakly dependent on concentration, this implies $J \sim n^{-1/3}$. Below T_{max}, ρ_2 is

Table 6. ρ_1 and ρ_2 as a function of n. ρ_1 is determined from zero field data. ρ_2 is determined for the field given in column 4

n (% Ce)	ρ_1 ($\mu\Omega$ - cm)	ρ_2 ($\mu\Omega$ - cm)	H for ρ_2 (Oe)
0.20	-.345	-	-
1.02	-.356	.109	6700
2.03	-.360	.106	3200
		.145	12000
3.23	-.417	.202	3200
3.98	-.462	.272	670

proportional to n^2, but an exact theoretical expression for the dependence of ρ_2 on n and J does not seem to exist, so not even a qualitative analysis can be made.

It should be observed that the above analysis for ρ_1 would imply according to Abrikosov's expression, $T_{max} \sim e^{-1/|J|}$ (22), that T_{max} should decrease as n increases, which is contrary to the experimental results. The fact that the data were taken in an external field is an added parameter not considered in the theory, but it is probably not responsible

for the discrepancy shown here. There appears to be no easy way to relate the J values determined from the ln T coefficients to T_{max}. The data are in good qualitative agreement with the ASK theory in that there is a distinct resonant like behavior with ln T approaches to the resonance. The behavior of T_{max}, however, would require that J increase slowly with concentration.

No attempt to compare the data with the localized spin fluctuation model was made since the existence of a maximum in ρ is catagorical evidence that it is not applicable for this system.

The traditional interpretation of T_{max} is to associate it with a classic ordering or Néel temperature, but for La-Ce this interpretation should be seriously questioned. A comparison of the present data with earlier work on more concentrated alloys of La-Ce indicates that there is no susceptibility change at T_{max}. In 1957 Roberts and Lock (57) measured the specific heat and the susceptibility of pure Ce and La-Ce alloys. For the pure Ce they found anomalies in the specific heat and the susceptibility at 12.5 K which they interpreted as an antiferromagnetic phase transition. When they began diluting the Ce with La, they found that the single specific heat anomaly separated into two anomalies, both of which moved to lower temperatures as the percent La was increased. The associated susceptibility measurements showed an antiferromagnetic transition which corresponded to the lower temperature specific heat anomaly, but showed absolutely nothing at the higher temperature anomaly. They were unable to give any satisfactory explanation of the upper specific heat anomaly. In 1969 Elliott, Hill and Miner (58) measured the resistivity of

a similar set of La-Ce alloys ranging from 27% to 91% Ce. A sharp change in slope similar to the one for pure Ce (see Appendix D) existed for each sample and was associated with the antiferromagnetic transition. They also observed a resistivity minimum just above the Néel temperature for samples containing 14, 16 and 18% La. This they interpreted as the first Kondo minimum seen in concentrated alloys. The interesting result of this work is that the Néel temperatures they determined resistively did not agree with those determined magnetically by Roberts and Lock (57). They, in fact, agreed with the temperature of the upper specific heat anomaly. The results were explained on the basis of a spin compensated state and not ordering effects.

The temperature associated with the lower specific heat and susceptibility anomalies extrapolates to zero at a Ce concentration of about 12%. The temperature associated with the upper magnetic transition extrapolates to zero for zero Ce concentration and is shown on Figure 22. T_{max} for the present data, extrapolated to zero field (Figure 23), are plotted on the same figure. These show reasonable agreement with the extrapolation of the resistive and upper specific heat transitions.

We suggest the following interpretation for these results. The lower temperature specific heat and susceptibility anomalies indicate an antiferromagnetic type transition. Below 12% Ce in La, this type of transition apparently can not take place. The magnetic transition associated with the upper specific heat anomalies and the resistivity measurements are associated with the formation of a resonant scattering state which may be similar to that outlined by the ASK theory. The absence of a susceptibility

anomaly associated with such a reasonant state is a little mysterious, but its absence from a resonant state makes more sense than its absence from a magnetic peak.

Superconducting Properties

Superconductivity was exhibited by all the samples measured. The zero field transitions shown in Figure 24 have widths which range from 0.15 K for the 1.0% sample to 0.6 K for the 4.0% sample. If all the broadening were caused by sample inhomogeneity, this would imply $\pm$ 10% and $\pm$ 13% inhomogeneities respectively in the distribution of Ce atoms. Another factor which might contribute to the width of the transition was stray fields from the superconducting magnet. Unfortunately the transitions for the 2.0, 3.2 and 4.0% samples may not have been taken in exactly zero field because the magnet had previously been run up to 12 KOe. We have no way to assess the field profile at the samples under these conditions, but it may be important. Hence some of this broadening for these samples may come from this field inhomogeneity.

T_c has been taken as the $\rho = 0$ value of the transition which has been determined by extrapolating the linear portion of the curve to zero. This point was chosen instead of the more standard half height because it agreed with the extrapolation of the critical field curves. The difference in T_c for $\rho = 0$ and $\rho = 1/2\ \rho_{max}$ increased as the impurity concentration increased and was .16 K for the 4.0% sample. This difference, however, made an insignificant change in the shape of the T_c versus n curve. The shape of the superconducting transition was also slightly dependent upon the

measuring current. A factor of 10 decrease in the current caused about a 0.05 K increase in T_c. This change can not be attributed to heating effects since above .1 K the resistivity is independent of current when the sample is completely normal. It should be noted that although the amount of fcc phase present in the samples is estimated to be less than 10%, the transition temperature may correspond to this phase and not the d-hcp phase of the bulk because filaments of superconducting fcc phase can short out the normal d-hcp.

The superconducting transition temperature was depressed sharply and almost linearly for increasing impurity concentration (Figure 25) with a slope of -1.27 K/wt. % Ce. In order to make a direct comparison with AG, T_c is also plotted on Figure 22 as T_c/T_{cp} where T_{cp} = 6.0 K is the transition temperature of pure lanthanum as determined by Finnemore et al. (59). The slope of the AG curve shown on the same figure is chosen arbitrarily to pass through the 1% Ce point. Above 1% Ce the data begin to deviate sharply from AG curve. This is not surprising, however, because AG theory assumes that the depression in T_c is caused by increased lifetime broadening only. The normal state properties already discussed indicate temperature dependent spin correlations, so the problem is certainly more complicated than AG.

Theoretical discussions of T_c versus n curves have been given by Bennemann (60), and he found that the localized spin fluctuation model gave deviations from the AG curve similar to the results here. Unfortunately not enough samples were studied to make a definitive statement about the concentration dependence of T_c.

Isothermal superconducting transitions for two of these samples are shown on Figures 26 and 27. Interpretation of these curves is always a little ambiguous, but the transitions aresimilar to the Nb transitions reported by Webb (61) for the same resistive AC measuring technique. For Nb, magnetization curves indicate that H_{c2} corresponded to the initial onset of resistance, and hence we have made the same interpretation here. H_{c3} is then taken to be the point where the normal state resistance is reached. For T/T_c between 0.3 and 1.0, the ratio of H_{c3}/H_{c2} is about 1.2 to 1.8. At lower temperatures H_{c3} is difficult to identify.

The critical field curves for H_{c2} are shown in Figure 28. The curves for .2% and 1% impurity show a region of distinct positive curvature as H approaches zero. Although this may be a real effect, it is most likely due to the small amount of fcc phase present in the predominantly d-hcp structure. That is to say, between the measured T_c and the temperature at which the bulk sample goes superconducting, about 1 K lower, the critical field is characteristic of the fcc filaments. When both phases become superconducting, the curves change character and appear to follow a critical field curve which extrapolates to T_c of the d-hcp phase. Since this behavior is not seen at higher concentrations this analysis implies that the difference in the critical fields for the two phases must become small.

Theoretical predictions for the critical field curves depend on the type of depairing mechanisms involved. The BCS prediction for the critical field of a pure type I superconductor with no depairing parameter is a family of nearly parabolic curves with H_c $(T = 0) \equiv H_o$ proportional to T_c.

If a temperature independent lifetime broadening, Γ, is the only depairing mechanism, as in AG for type I, then the curves are still nearly parabolic, but H_o decreases more rapidly than T_c. For type II materials, two depairing mechanisms are at work, H and Γ, and H_o/T_c is even lower than for AG. If in addition to H and Γ the sample also exhibits magnetic order, the critical field curves become very complicated as discussed by Bennemann, Garland and Mueller (62). A comparison of the experimental results with the double pair breaking theory is shown on Figure 28 for the 2% sample. The data fall considerably below the theoretical curve, and the difference is attributed to the exchange field enhancement effect as discussed by Bennemann et al. (62).

Near T_c the slope of these critical field curves (assuming an extrapolated d-hcp critical field for the 0.2 and 1% samples) show a striking resemblance to results reported for $La_{3-x}Gd_xAl$ (63). H_o seems to be independent of whether the impurity - conduction electron coupling (J) is ferromagnetic or antiferromagnetic for La - X alloys where X is a rare earth impurity. Figure 29 shows H_o as a function of T_c for $La_{98}La_{2-x}Tb_x$ (39,64) $La_{3-x}Gd_xAl$ (63) and La-Ce alloys. For Tb and Gd, J is assumed to be positive, while for Ce it is assumed to be negative. The fact that the exchange enhancement effect appears to be independent of the sign of J may prove valuable in understanding these systems.

It should be noted that the shape of the La-Lu-Tb critical field curves is different from the other two in that they rise much more quickly near T_c. They also level off and show a slight reentrant behavior, while the others do not. ($La_{3-x}Gd_x$ alloys, as measured by Crow et al. (65),

show a considerable reentrant behavior.) These differences in the character of the critical field curves probably reflect the fact that Gd and Tb show magnetic order whereas Ce shows a resonant scattering.

It is important to note that the La-Ce critical field curves to not change character as the temperature is lowered through the normal state resistivity maximum. If the maximum in the normal state resistivity were due to magnetic ordering of the Ce impurities, some change in the critical field curves at T_{max} would be expected. Hence, the fact that they are perfectly smooth through this region is strong evidence that the maximum in ρ_m is not caused by ordering of the Ce ions. Rather we attribute the maximum in ρ_m to the resonant character of the impurity scattering.

SUMMARY

Cerium impurities in lanthanum appear to maintain a moment over the entire temperature range from 0.060 K to 20.0 K and show no sign of the spin compensated state. Instead, the magnetic scattering has a resonant character with a logarithmic temperature dependence both above and below the resonance.

Both T_{max} and the slope of the resistivity below T_{max} increase approximately with the square of the concentration, as might be expected if two near neighbor Ce atoms were required for the interaction. In addition, T_{max} goes as $\mu \cdot H/k$ as would be expected from the Zeeman splitting. At temperatures above the maximum there does not seem to be a strong concentration dependence. If the data above T_{max} are analyzed in terms of the simple Kondo picture, the effective interaction constant, J, seems to decrease with concentration to maintain the coefficient of the ln T term independent of n.

The superconducting state data show that there is clear evidence of exchange enhancement for Ce in La. The fact that it is of about the same magnitude as for Tb and Gd might not have been expected beforehand since for Ce, J is negative and for Tb and Gd it is positive.

Probably the most interesting aspect of the superconducting state data is that the critical field curves do not change character as the normal state resistance proceeds through the resonance. This is a little surprising. It implies that the lifetime of the Cooper pairs due to spin scattering (Γ) does not change radically through the normal state resonance. One possible explanation might be that the normal state resonance is

governed by the s-f interaction whereas the superconductivity is controlled by the d-f interaction. If this were true it would be strong evidence that in La the electron-phonon interaction responsible for superconductivity is dominated by electrons with predominantly d-like character.

BIBLIOGRAPHY

1. G. J. van den Berg, in Progress in Low Temperature Physics (North-Holland Publishing Company, Amsterdam, 1964), Vol. IV.

2. A. J. Heeger, in Solid State Physics (Academic Press, New York, 1969) Vol. XXIII.

3. J. Kondo, in Solid State Physics (Academic Press, New York, 1969) Vol. XXIII.

4. M. D. Daybell and W. A. Steyert, Rev. Mod. Phys. 40, 380 (1968).

5. W. Meissner and G. Voigt, Ann. Phys. 1, 761, 892 (1930).

6. W. J. de Haas, J. H. de Boer and G. J. van den Berg, Physica 1, 1115 (1933-1934).

7. A. N. Gerritsen and J. O. Linde, Physica 17, 573 (1951).

8. W. B. Pearson, Phil. Mag. 46, 911, 920 (1955).

9. A. Kjekshus and W. B. Pearson, Can. J. Phys. 40, 98 (1962).

10. A. N. Gerritsen and J. O. Linde, Physica 18, 877 (1952).

11. A. N. Gerritsen and J. O. Linde, Physica 17, 573 (1951).

12. T. Sugawara, J. Phys. Soc. Japan 20, 2252 (1965).

13. T. Sugawara and H. Eguchi, J. Phys. Soc. Japan 26, 1322 (1969).

14. T. Sugawara and H. Eguchi, J. Phys. Soc. Japan 21, 725 (1966).

15. D. T. Peterson, D. F. Page, R. B. Rump, and D. K. Finnemore, Phys. Rev. 153, 701 (1967).

16. A. D. Caplin and C. Rizzuto, Phys. Rev. Letters 21, 746 (1968).

17. P. W. Anderson, Phys. Rev. 124, 41 (1961).

18. J. Kondo, Progr. Theoret. Phys. 32, 37 (1964).

19. J. Kondo, Prog. Theoret. Phys. 36, 429 (1966); Phys. Rev. 154, 644 (1967).

20. K. Yosida, Phys. Rev. 147, 223 (1966); Prog. Theoret. Phys. 36, 875 (1966).

21. Y. Nagaoka, Phys. Rev. 138, 1112 (1965).

22. A. A. Abrikosov, Physica 2, 5 (1965).

23. H. Suhl, Phys. Rev. 138, A515 (1965); Phys. Rev. 141, 483 (1966); Physics 2, 39 (1965).

24. J. Kondo, Progr. Theoret. Phys. 40, 695 (1968).

25. H. Suhl, Phys. Rev. Letters 19, 442 (1967).

26. M. J. Levine, T. V. Ramakrishnan, and R. A. Weiner, Phys. Rev. Letters 20, 1370 (1968).

27. J. Bardeen, L. N. Cooper, and J. R. Schrieffer, Phys. Rev. 108, 1175 (1957).

28. A. A. Abrikosov and L. P. Gor'kov, Zh. Eksperim. i Teor. Fiz. 39, 1781 (1960) [English transl.: Soviet Phys.--JETP 12, 1243 (1961)].

29. F. Reif and M. A. Woolf, Phys. Rev. Letters 9, 315 (1962).

30. J. Millstein and M. Tinkham, Phys. Rev. 158, 325 (1967).

31. W. R. Decker and D. K. Finnemore, Phys. Rev. 172, 430 (1968).

32. M. B. Maple, Phys. Letters, 26A, 513 (1968).

33. B. T. Matthias, H. Suhl, and E. Corenzwit, Phys. Rev. Letters 1, 92 (1958).

34. R. A. Hein, R. L. Falge, Jr., B. T. Matthias, and E. Corenzwit, Phys. Rev. Letters 2, 500 (1959).

35. J. E. Crow and R. D. Parks, Phys. Letters 21, 378 (1966).

36. K. H. Bennemann, Phys. Rev. Letters 17, 438 (1966).

37. P. Fulde and K. Maki, Phys. Rev. 141, 275 (1966).

38. K. H. Bennemann, J. W. Garland, and F. M. Mueller, Phys. Rev. Letters 23, 169 (1969).

39. L. J. Williams, W. R. Decker and D. K. Finnemore, (to be published in Phys. Rev.).

40. K. H. Bennemann, Phys. Rev. 183, 492 (1969).

41. M. B. Maple, J. G. Huber, B. R. Coles, and A. C. Lawson, (to be published).

42. J. C. Wheatley, O. E. Vilches, and W. R. Abel, Physica 4, 1 (1968).

43. Ray Radebaugh, Thermodynamic Properties of He^3-He^4 Solutions with Applications to the He^3-He^4 Dilution Refrigerator, NBS Technical Note No. 362 (1967).

44. J. C. Wheatley, Am. J. Phys. 36, 181 (1968).

45. W. R. Abel, A. C. Anderson, W. C. Black, and J. C. Wheatley, Physics 1, 337 (1965).

46. J. M. Daniels and F. N. H. Robinson, Phil. Mag. 44, 630 (1953).

47. E. N. Hopkins, D. T. Peterson, and H. H. Baker (to be published).

48. A. Matthiessen, Rep. Brit. Ass. 32, 144 (1862).

49. N. F. Mott, Advan. Phys. 13, (1964).

50. W. G. Baber, Proc. Roy. Soc. A158, 383 (1937).

51. G. K. White and R. J. Tainsh, Phys. Rev. Letters 19, 165 (1967).

52. A. H. Wilson, Proc. Roy. Soc. A167, 580 (1938).

53. N. F. Mott, Proc. Roy. Soc. A153, 699 (1935).

54. J. M. Ziman, Electrons and Phonons (Oxford University Press, London, 1960).

55. S. Arajs and E. E. Anderson, J. Appl. Phys. 40, 1470 (1969).

56. M. B. Maple and Z. Fisk, in Proceedings of the Eleventh International Conference on Low Temperature Physics, St. Andrews, Scotland, 1968, edited by D. M. Findlayson and D. M. McCall (St. Andrews University Press, St. Andrews, Scotland, 1968).

57. L. M. Roberts and J. M. Lock, Phil. Mag. 2, 811 (1957).

58. R. O. Elliott, H. H. Hill, and W. N. Miner, Phys. Stat. Sol. 32, 609 (1969).

59. D. K. Finnemore, D. L. Johnson, J. E. Ostenson, F. H. Spedding, and B. J. Beaudry, Phys. Rev. 137, A550 (1965).

60. K. H. Bennemann, Phys. Rev. 183, 492 (1969).

61. G. W. Webb, Solid State Commun. 6, 33 (1968).

62. K. H. Bennemann, J. W. Garland, and F. M. Mueller, Phys. Rev. Letters 23, 169 (1969).

63. Y. Kuwasawa, K. Sekizawa, N. Usui, and K. Yasukochi, J. Phys. Soc. Japan 27, 590 (1969).

64. W. J. Keeler, and H. L. Watson, (private communication).

65. J. E. Crow, R. P. Guertin, and R. D. Parks, Phys. Rev. Letters 19, 77 (1967).

ACKNOWLEDGMENTS

The author thanks Dr. D. K. Finnemore for his active interest in this research project and for his help in preparing this manuscript.

He would also like to thank Mr. J. E. Ostenson for helping set up the apparatus, Mr. R. Delfs for assisting in construction and in thermometry calibration, Mr. H. L. Watson for making and preparing the samples, and to all members of his group for helpful and interesting conversations through the years.

Finally, special thanks are extended to Drs. D. K. Finnemore, C. A. Swenson and D. J. Zaffarano for their aid in finding future employment for the author.

FIGURES

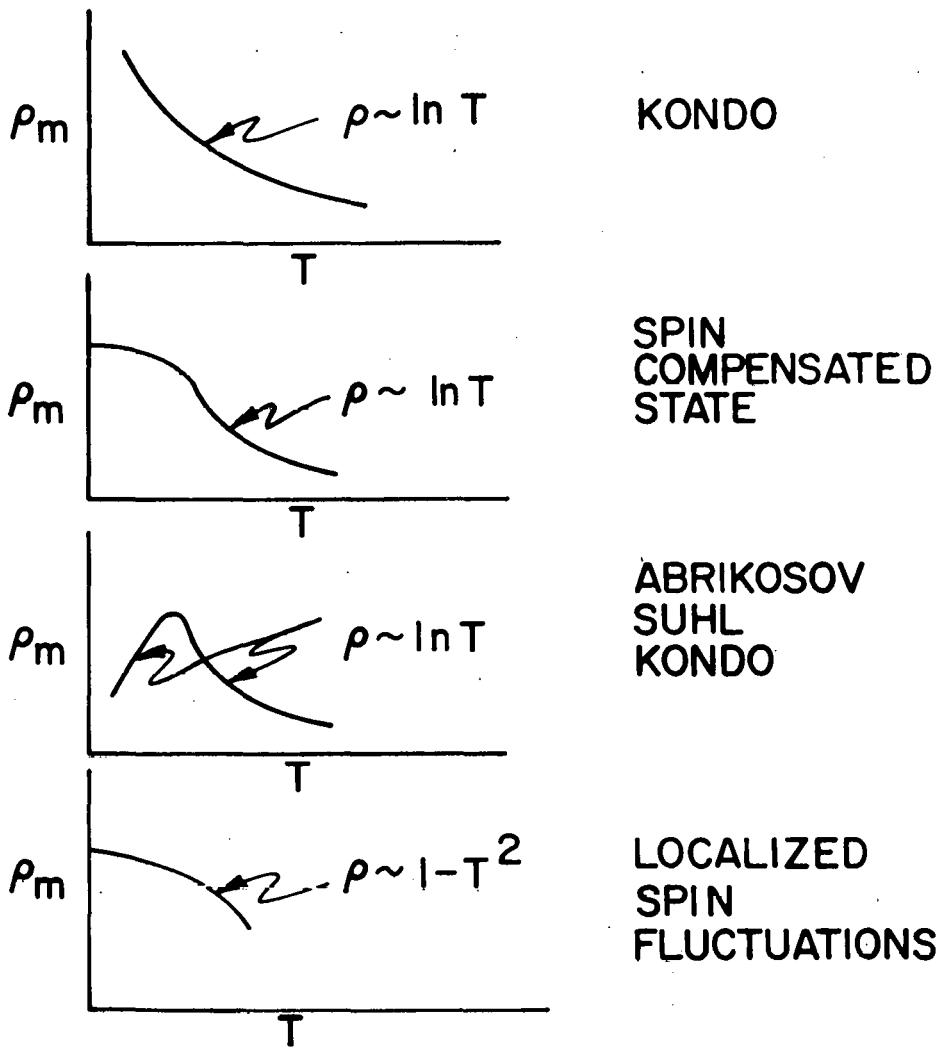

Figure 1. The various theoretical predictions of ρ_m, the magnetic contribution to the resistivity, as a function of temperature.

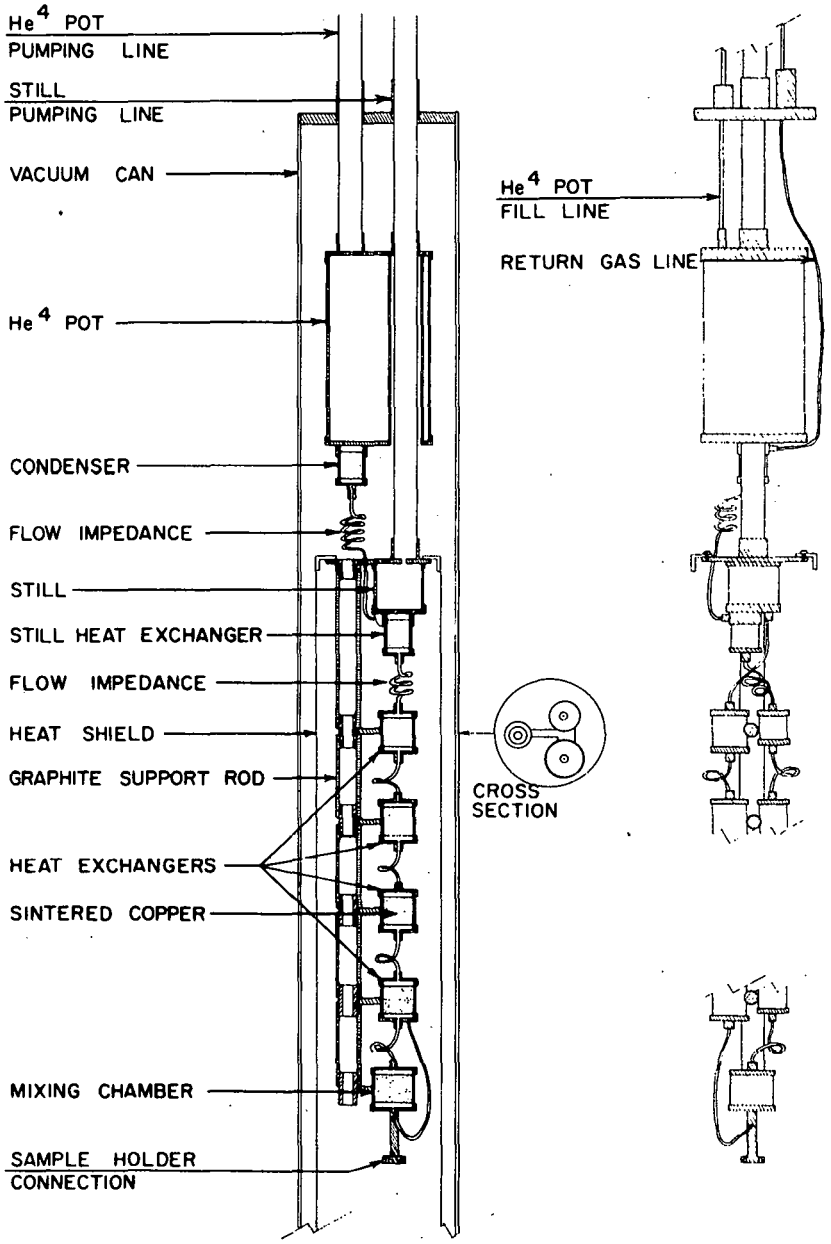

Figure 2. A cutaway drawing of the He^3-He^4 dilution refrigerator on the left and a side view on the right.

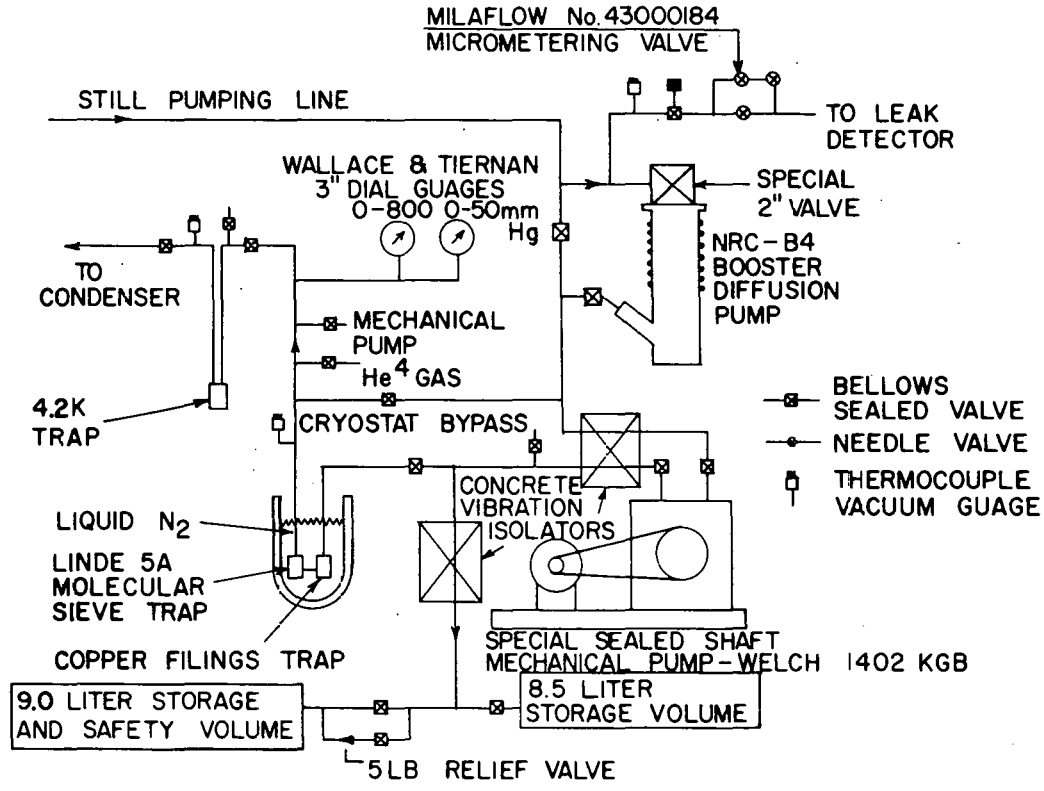

Figure 3. The external gas circulation and storage system.

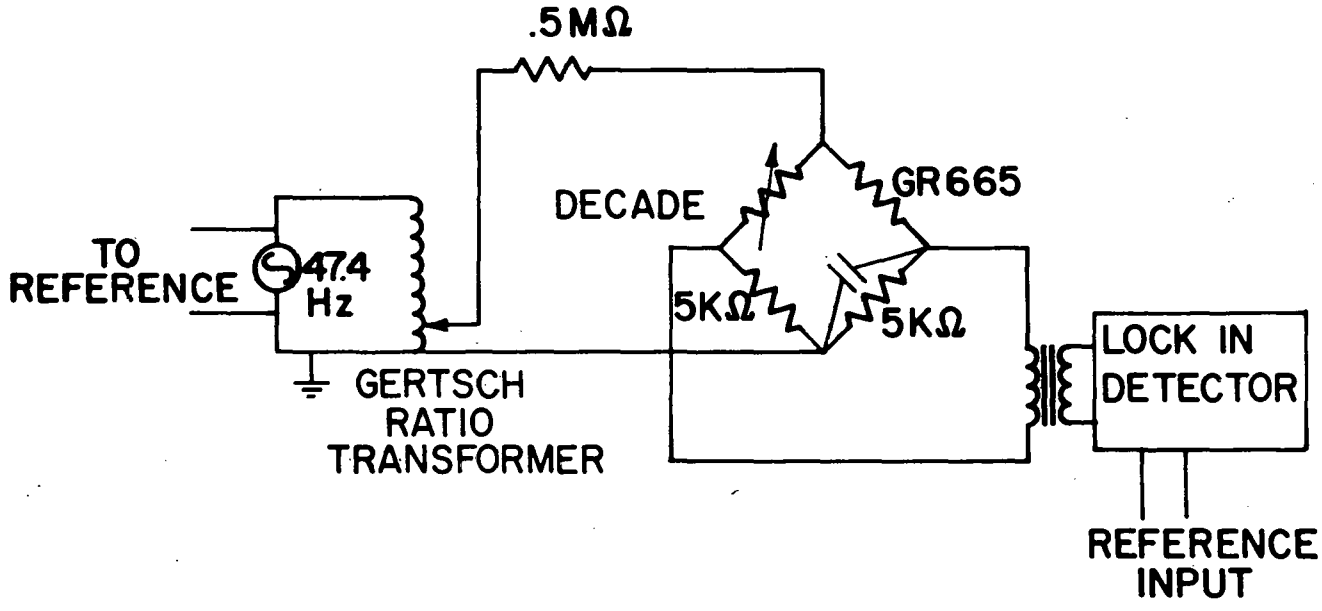

Figure 4. 47.4 Hz Whetstone bridge.

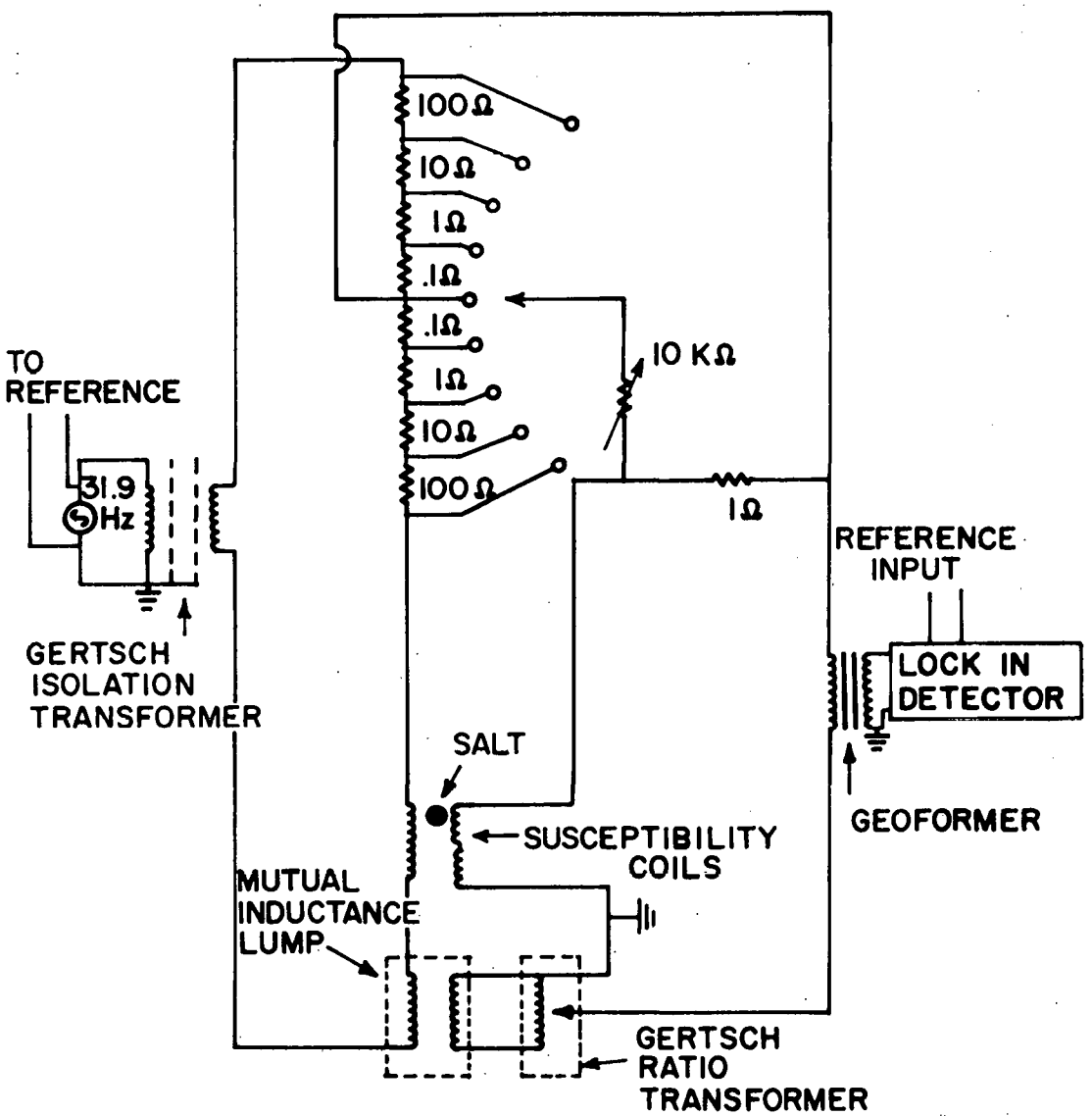

Figure 5. 31.9 Hz mutual inductance bridge.

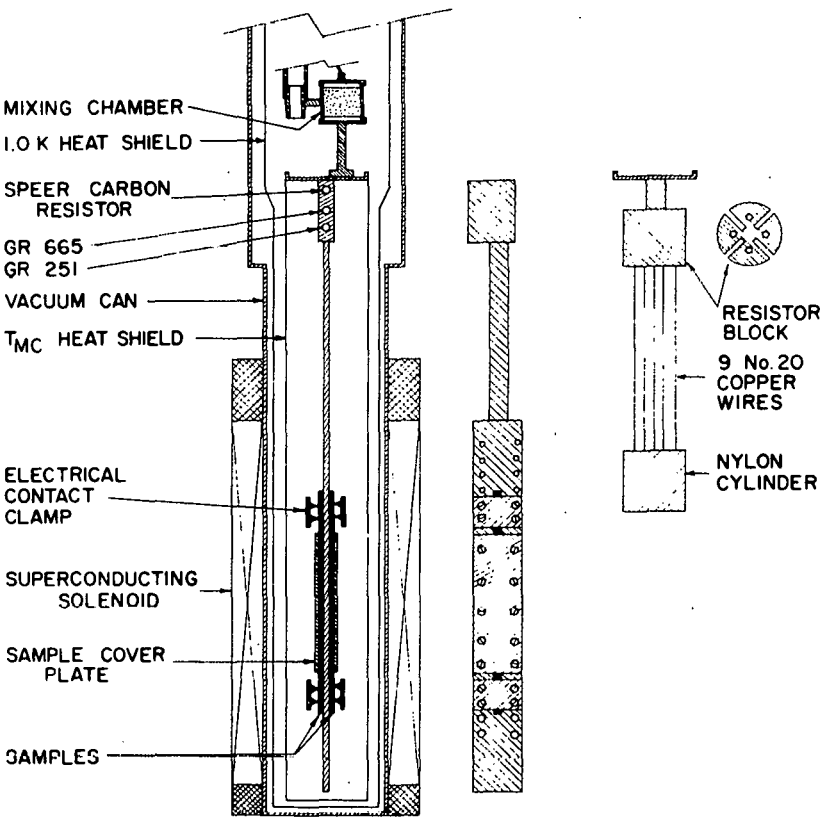

Figure 6. Details of the sample holder on the left and thermometer calibration apparatus on the right.

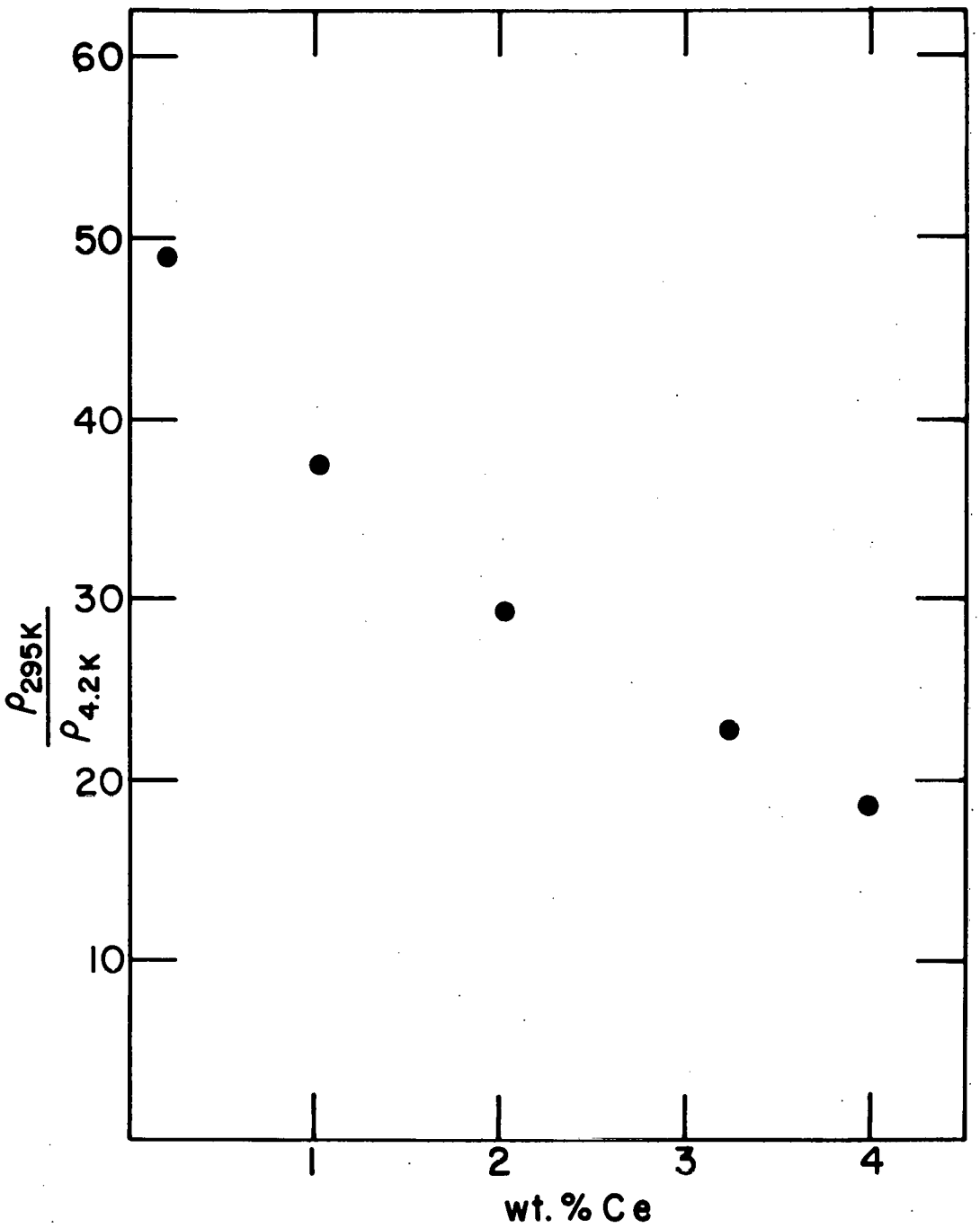

Figure 7. The resistivity ratio, $\rho(T = 295\ K)/\rho(T = 4.2\ K)$, as a function of cerium concentration.

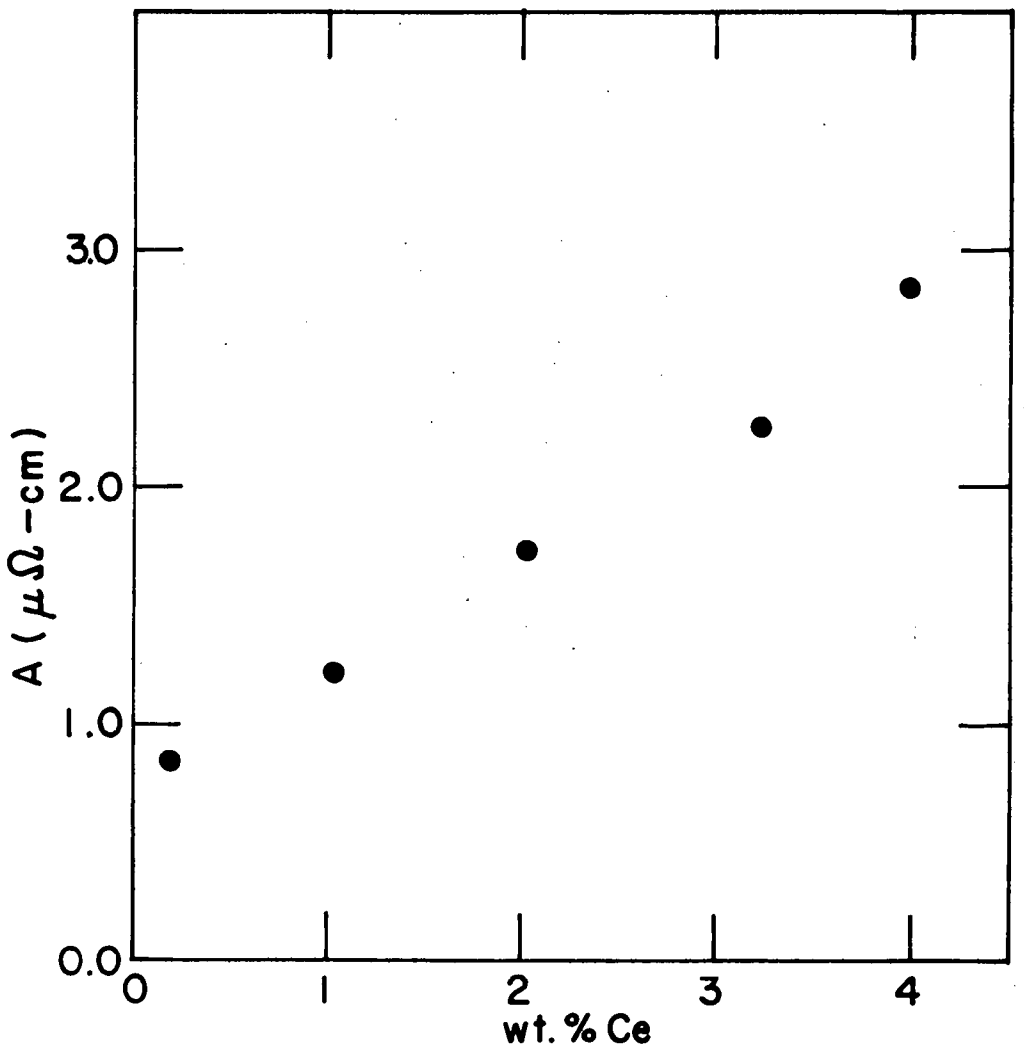

Figure 8. The temperature independent resistivity, A, as a function of cerium concentration, where A is determined from the high temperature fit, $\rho_o = A + BT^{2.25}$.

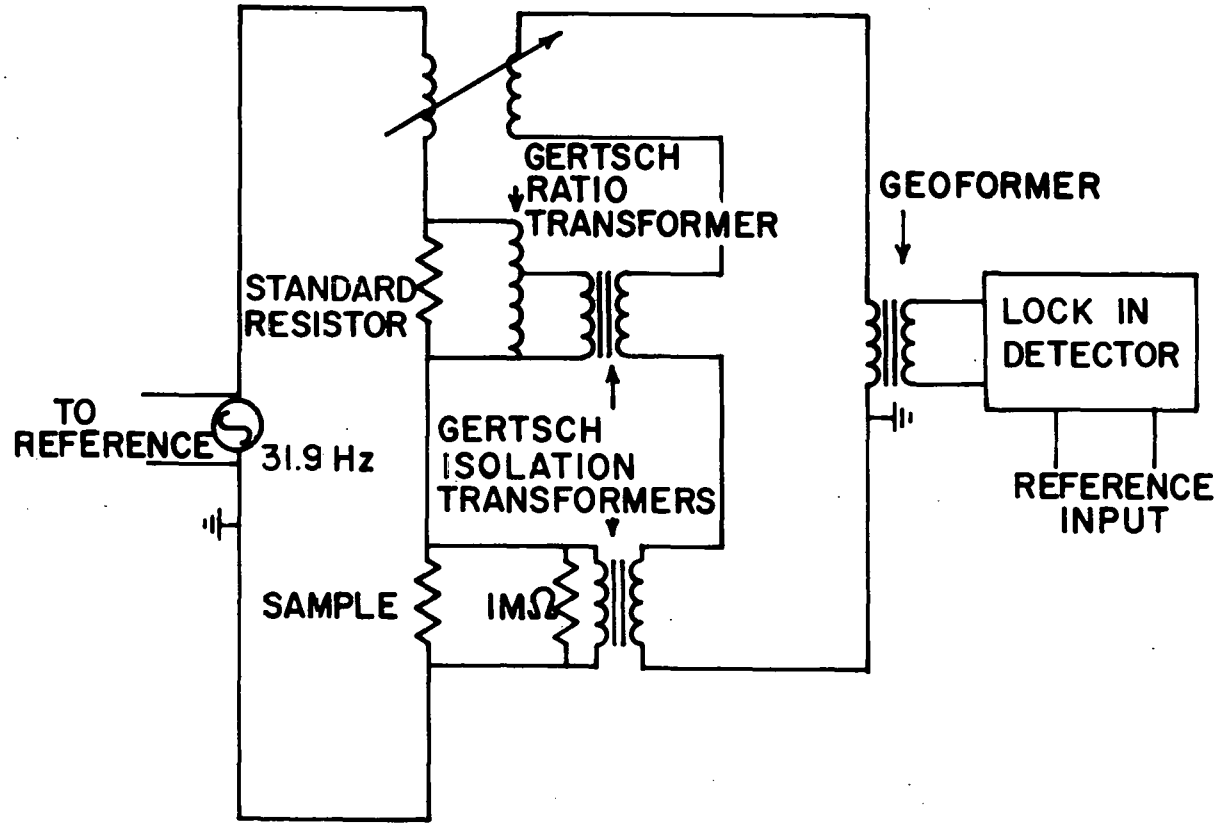

Figure 9. The sample resistance measuring bridge.

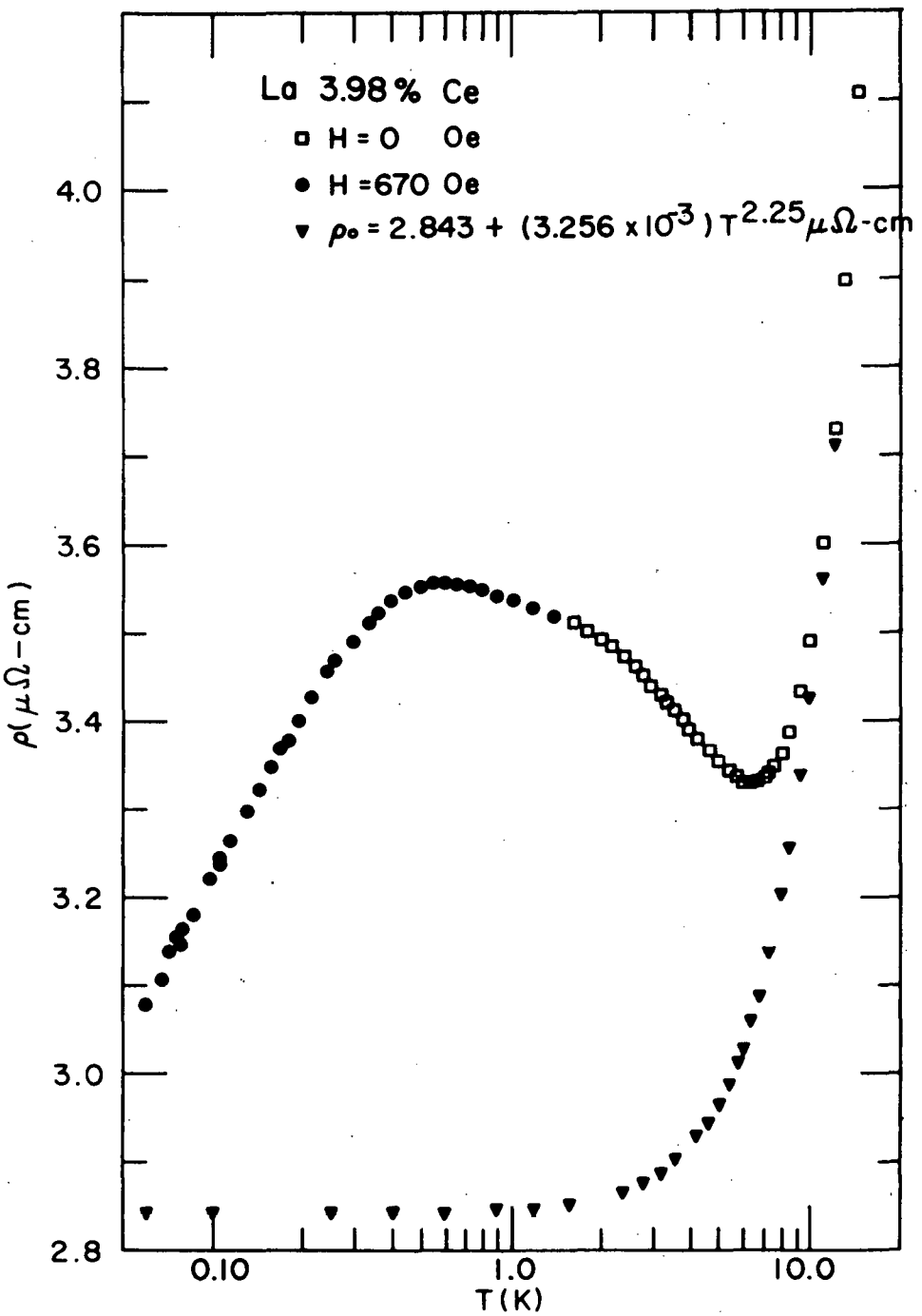

Figure 10. The normal state resistivity La 4.0 wt. % Ce and the extrapolation of the high temperature fit $\rho_o = A + BT^{2.25}$.

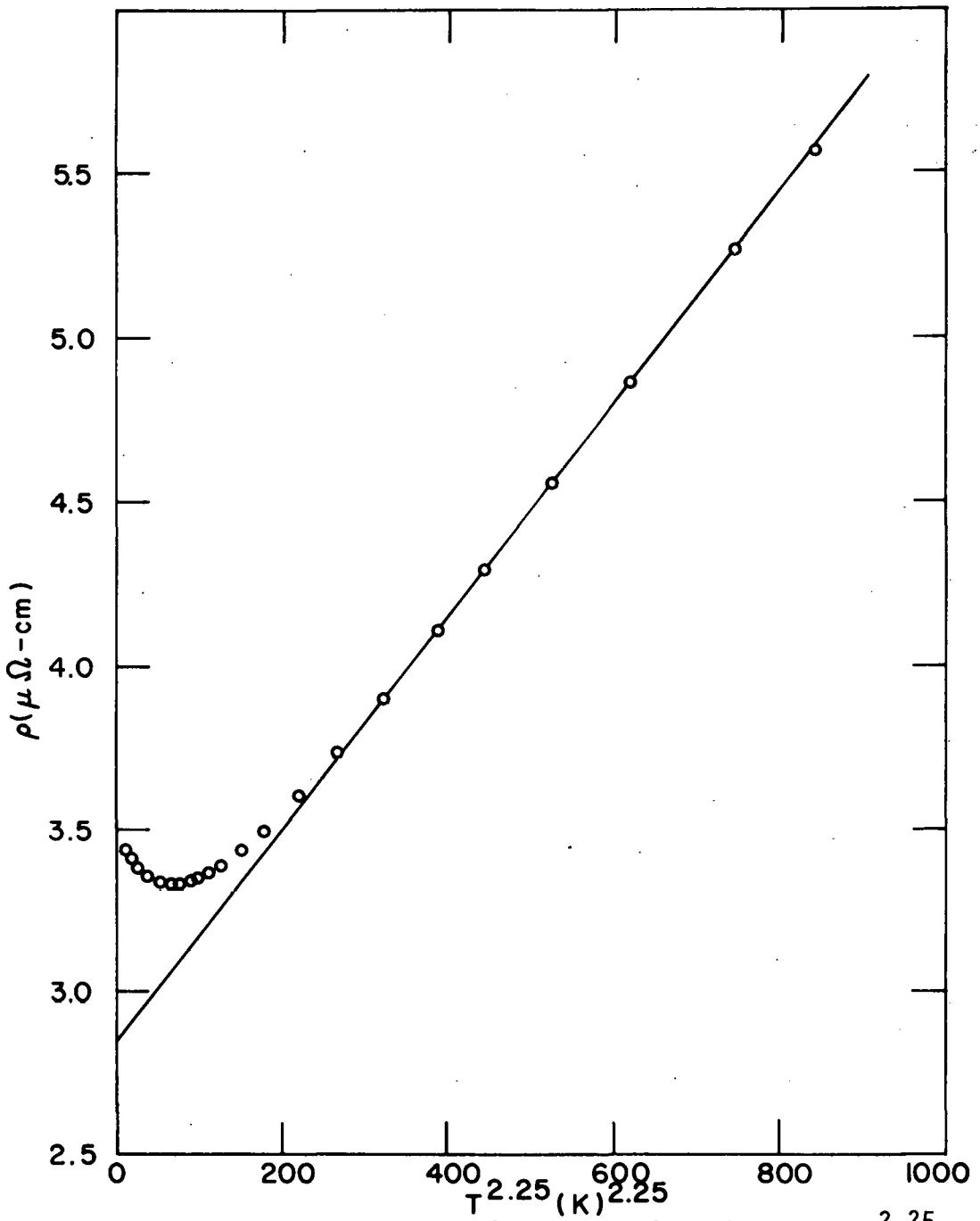

Figure 11. The resistivity of La 3.98 wt. % Ce fitted to $A + BT^{2.25}$.

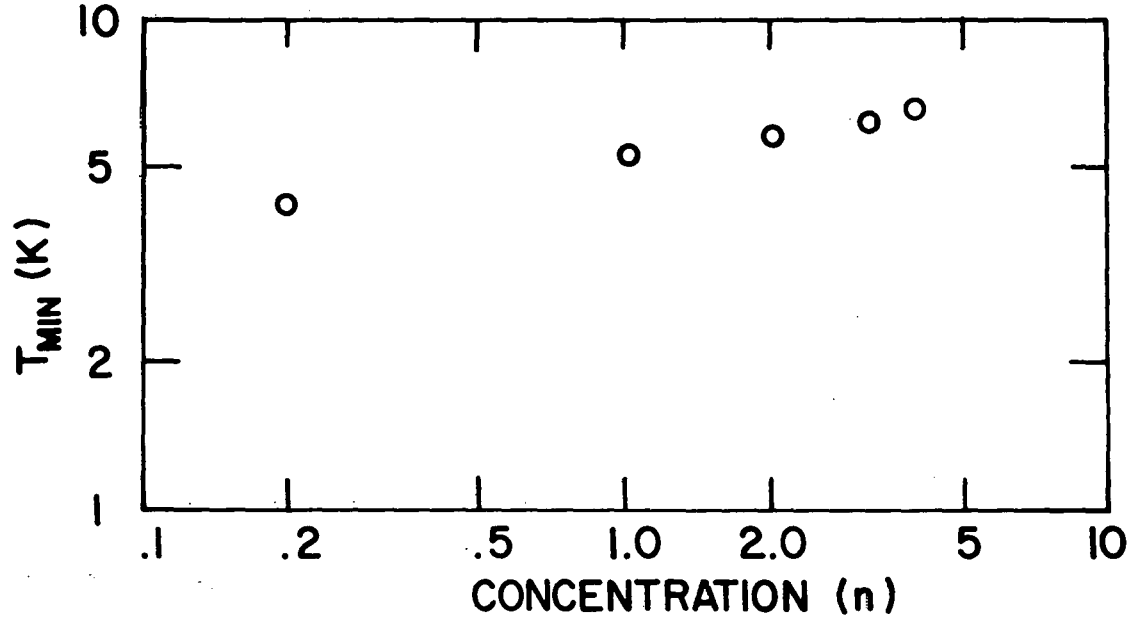

Figure 12. The minimum temperature, T_m, in the normal state resistivity as a function of cerium impurity.

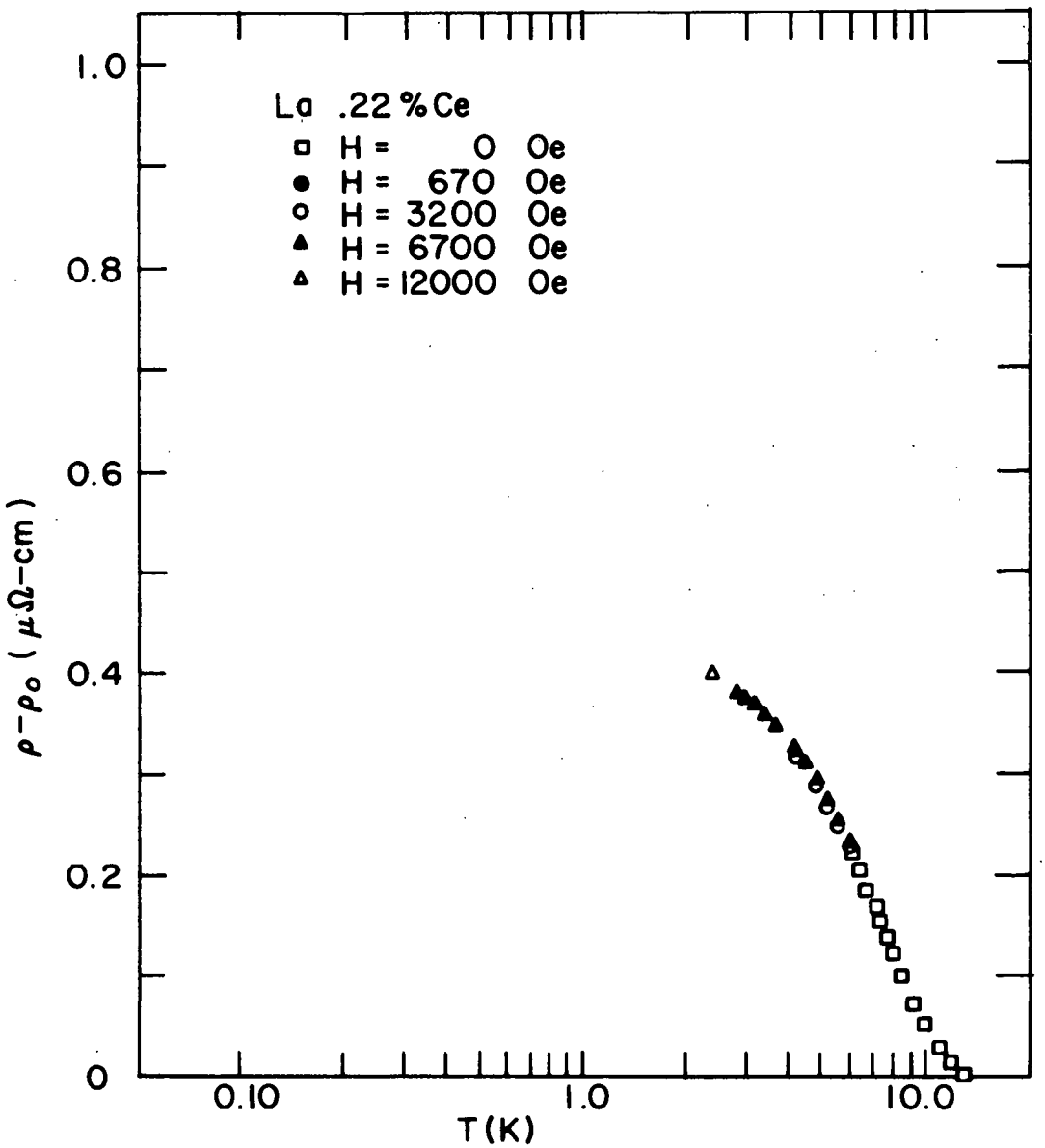

Figure 13. The magnetic scattering contribution to the resistivity, ρ_m, for La .22 % Ce.

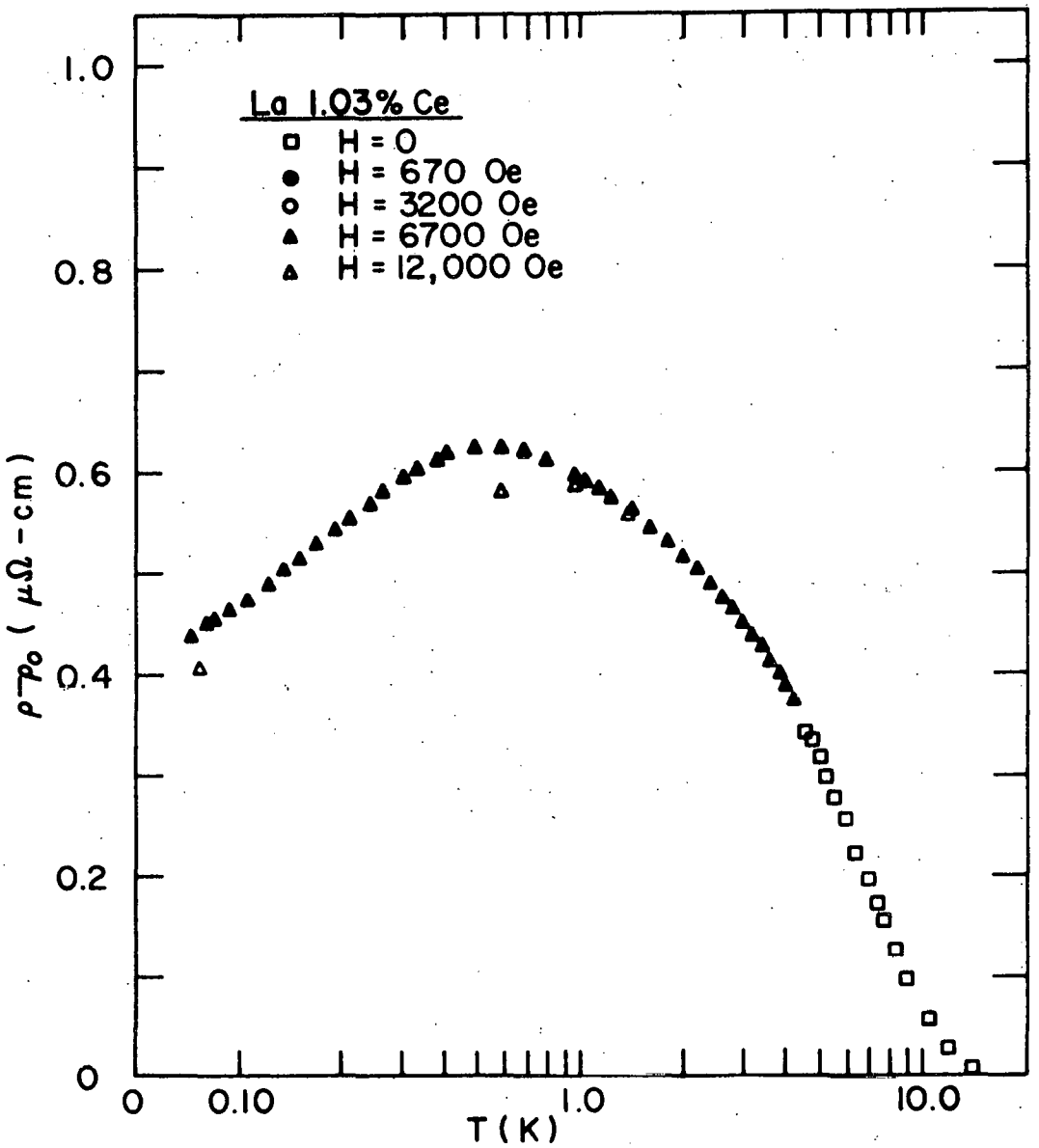

Figure 14. The magnetic scattering contribution to the resistivity, ρ_m, for La 1.03 % Ce.

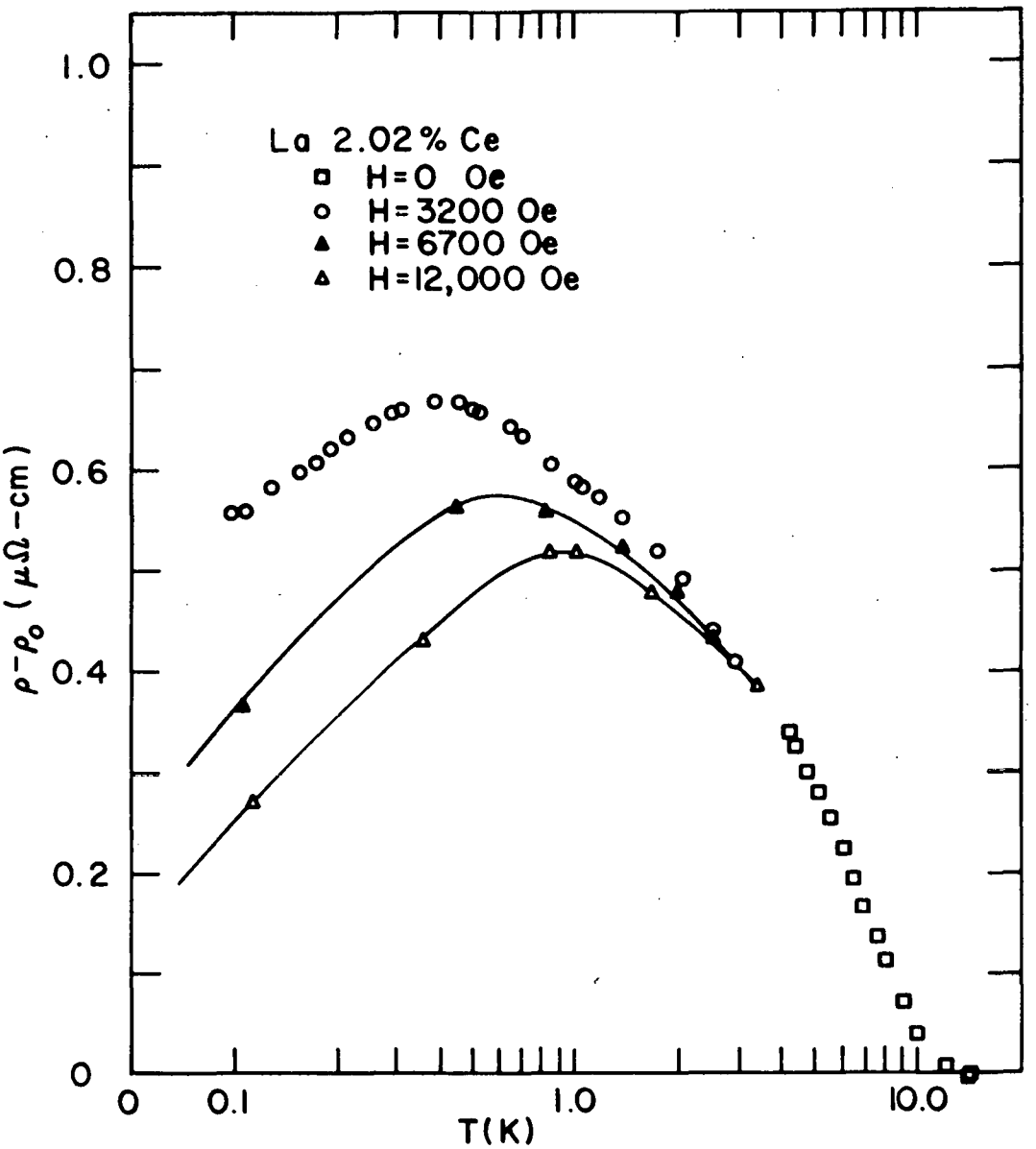

Figure 15. The magnetic scattering contribution to the resistivity, ρ_m, for La 2.02 % Ce.

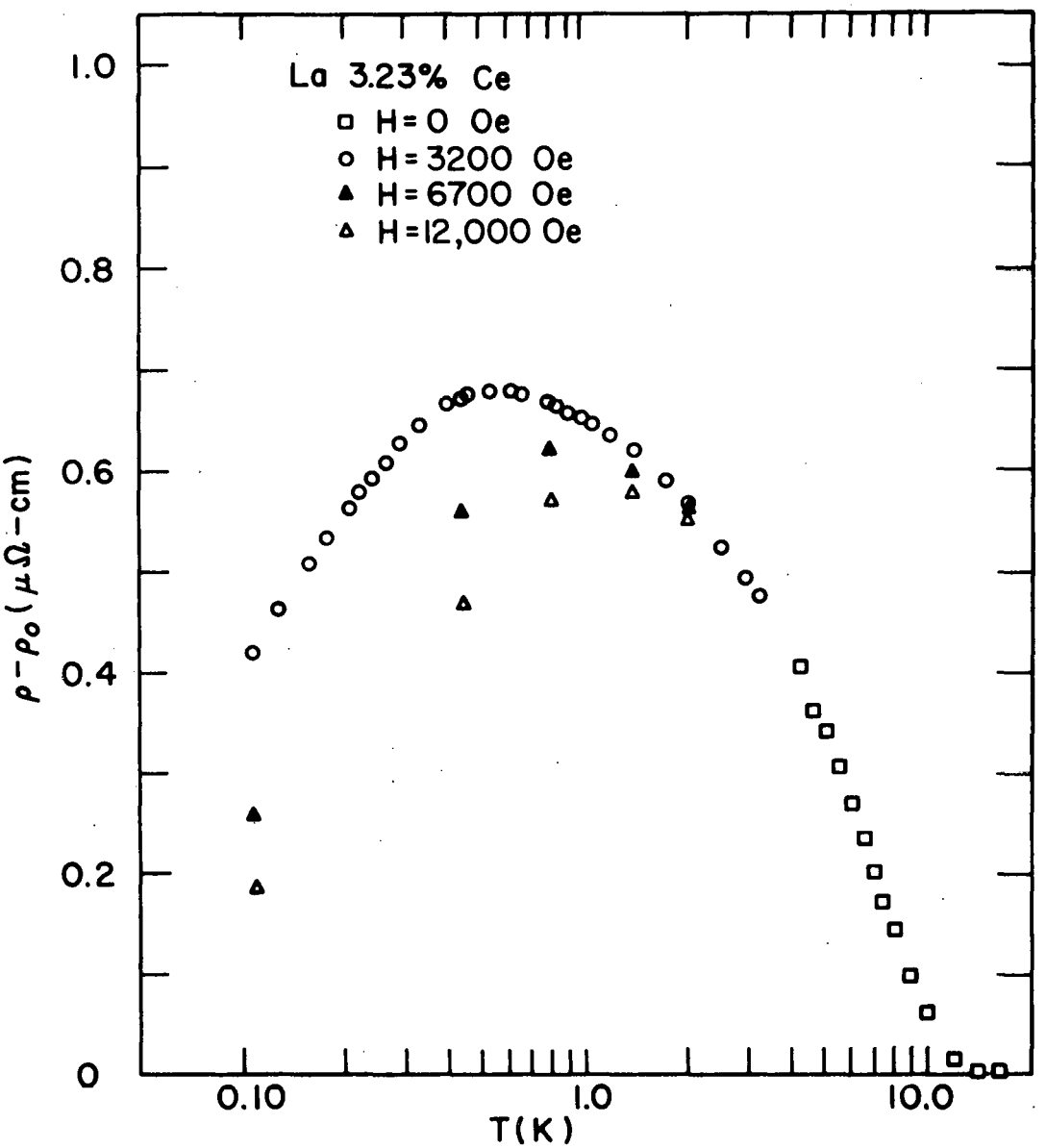

Figure 16. The magnetic scattering contribution to the resistivity, ρ_m, for La 3.23 % Ce.

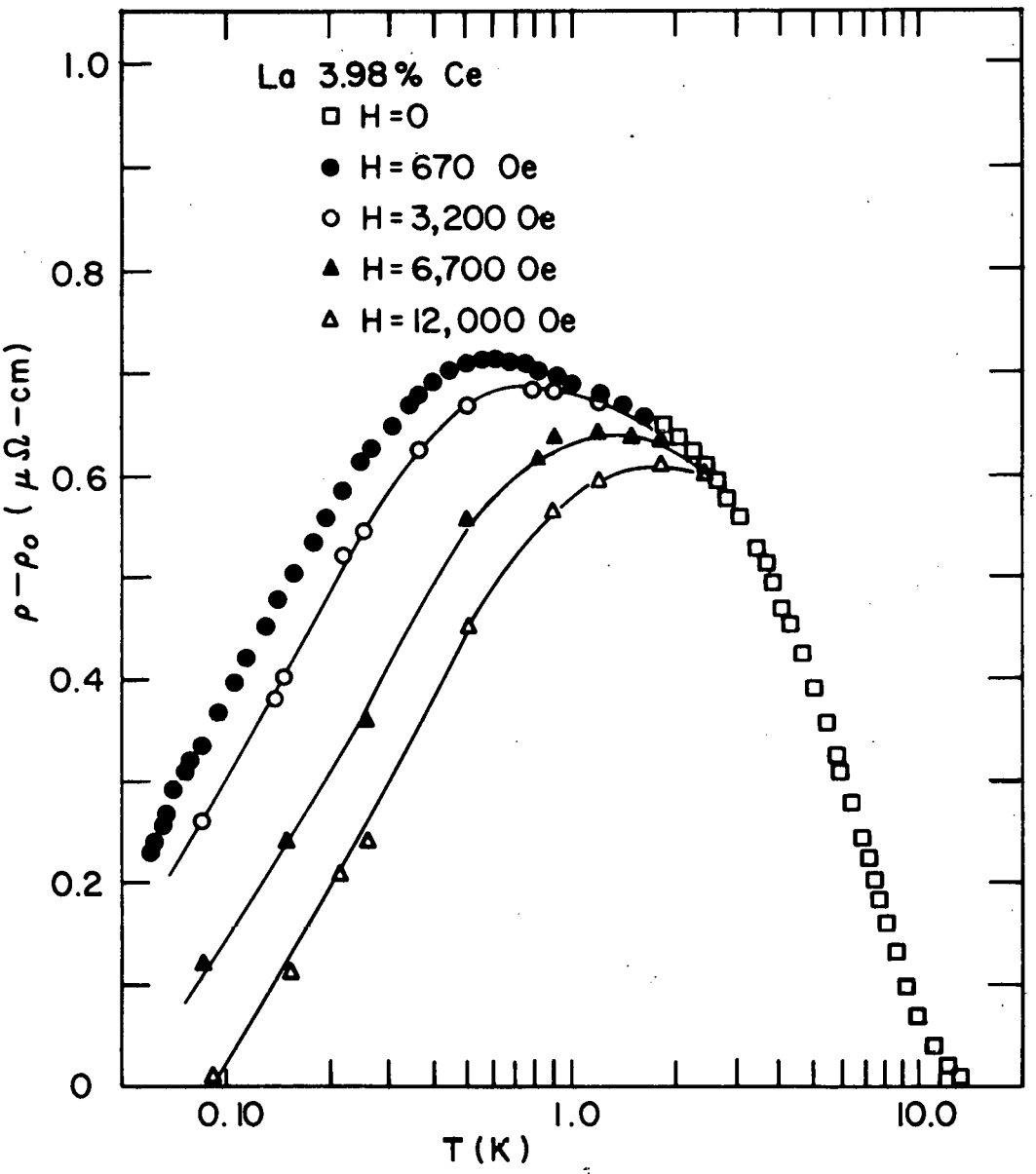

Figure 17. The magnetic scattering contribution to the resistivity, ρ_m, for La 3.98 % Ce.

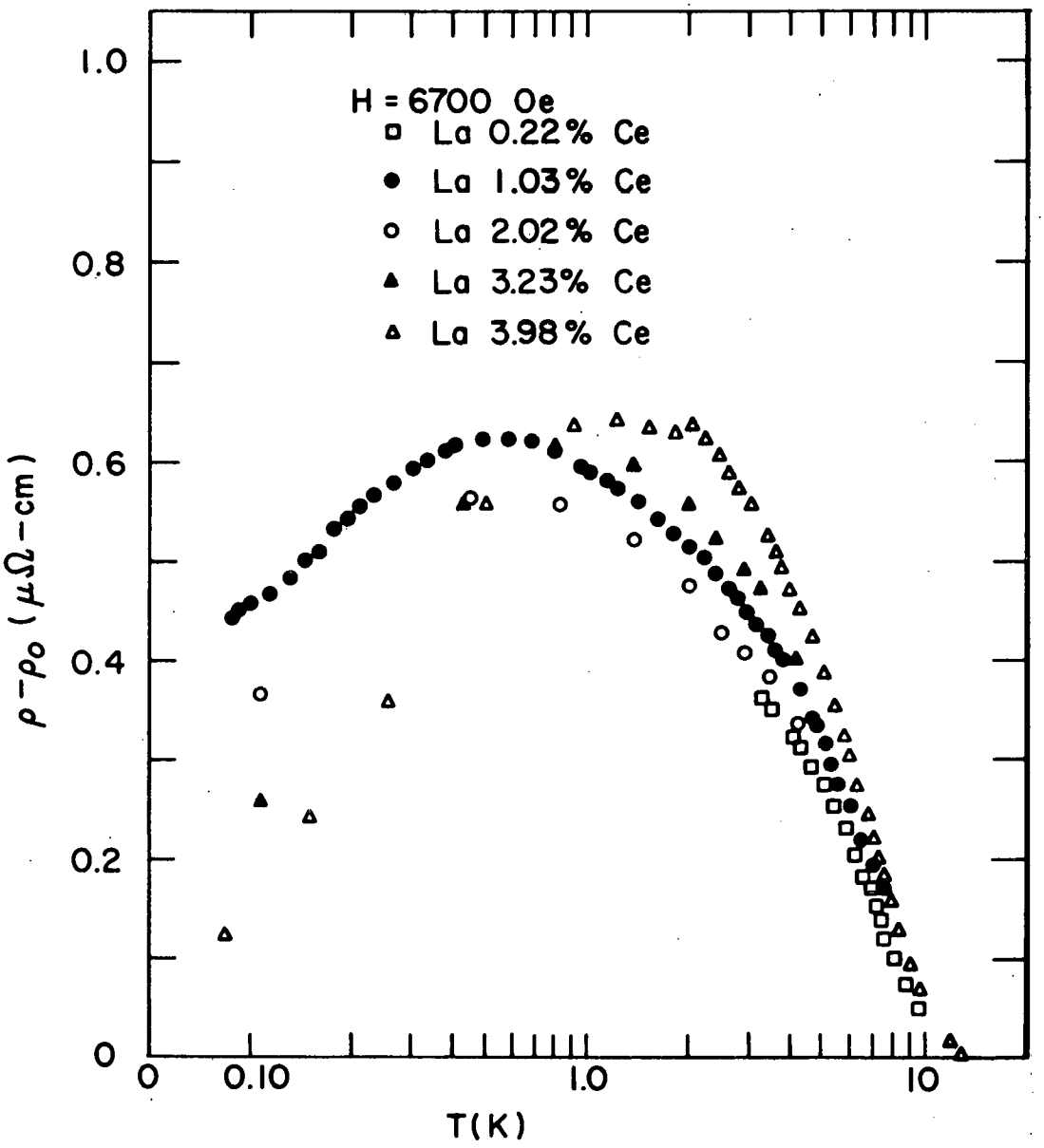

Figure 18. ρ_m for the five samples at H = 6700 Oe.

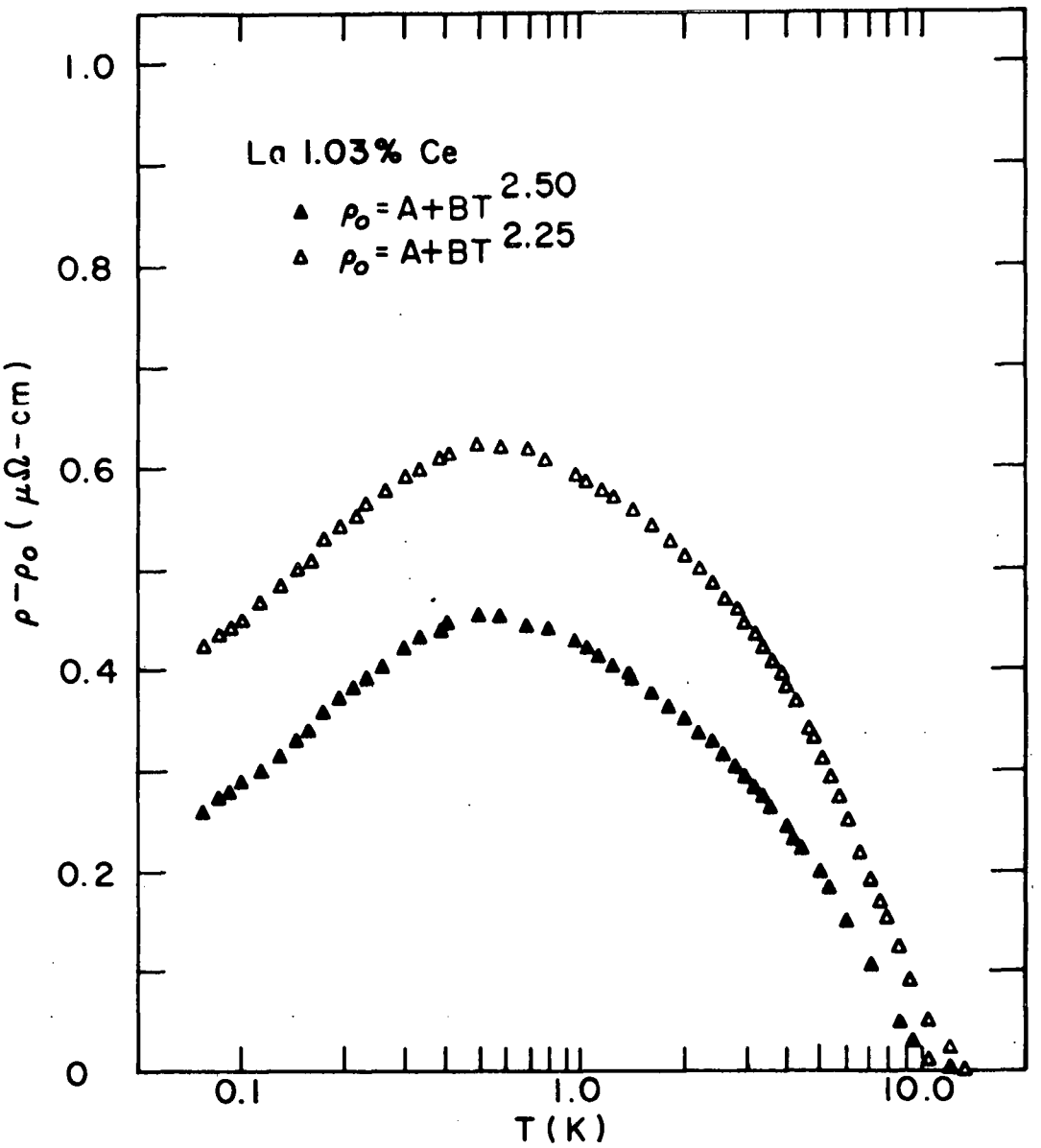

Figure 19. The change in ρ_m for La 1.03 % Ce as the temperature dependence of ρ_o is changed from $T^{2.25}$ to $T^{2.50}$.

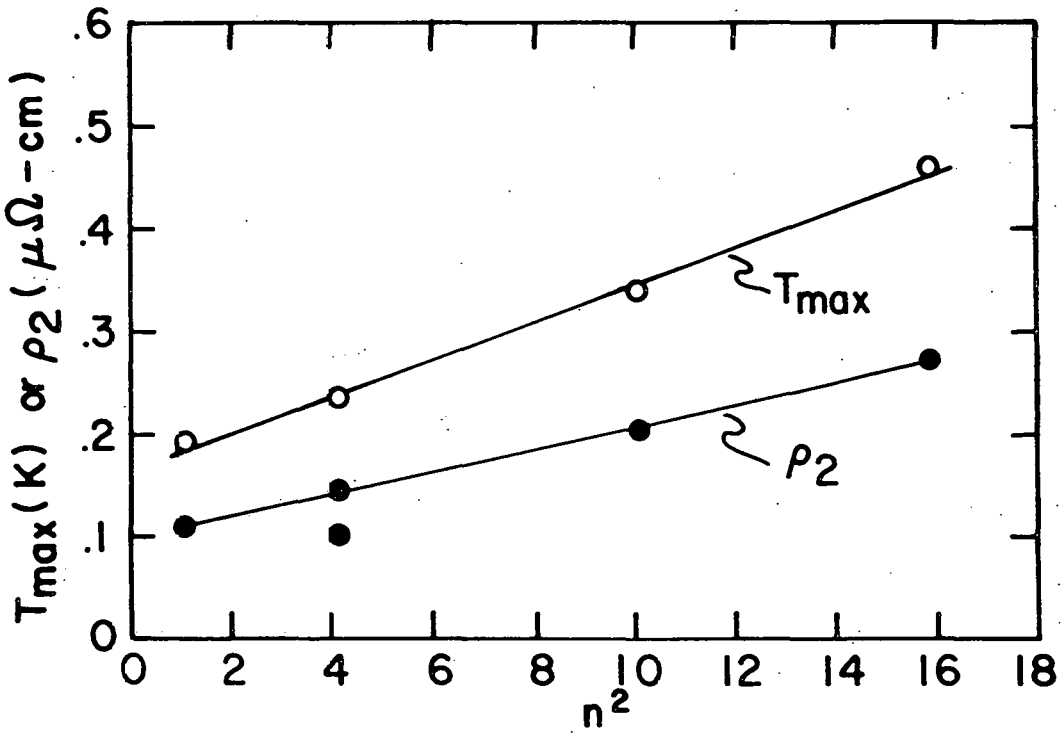

Figure 20. The concentration dependence of the temperature of the maximum, $T_{max}(H=0)$, in the normal state resistivity and the slope, ρ_2, of the ln T below T_{max}.

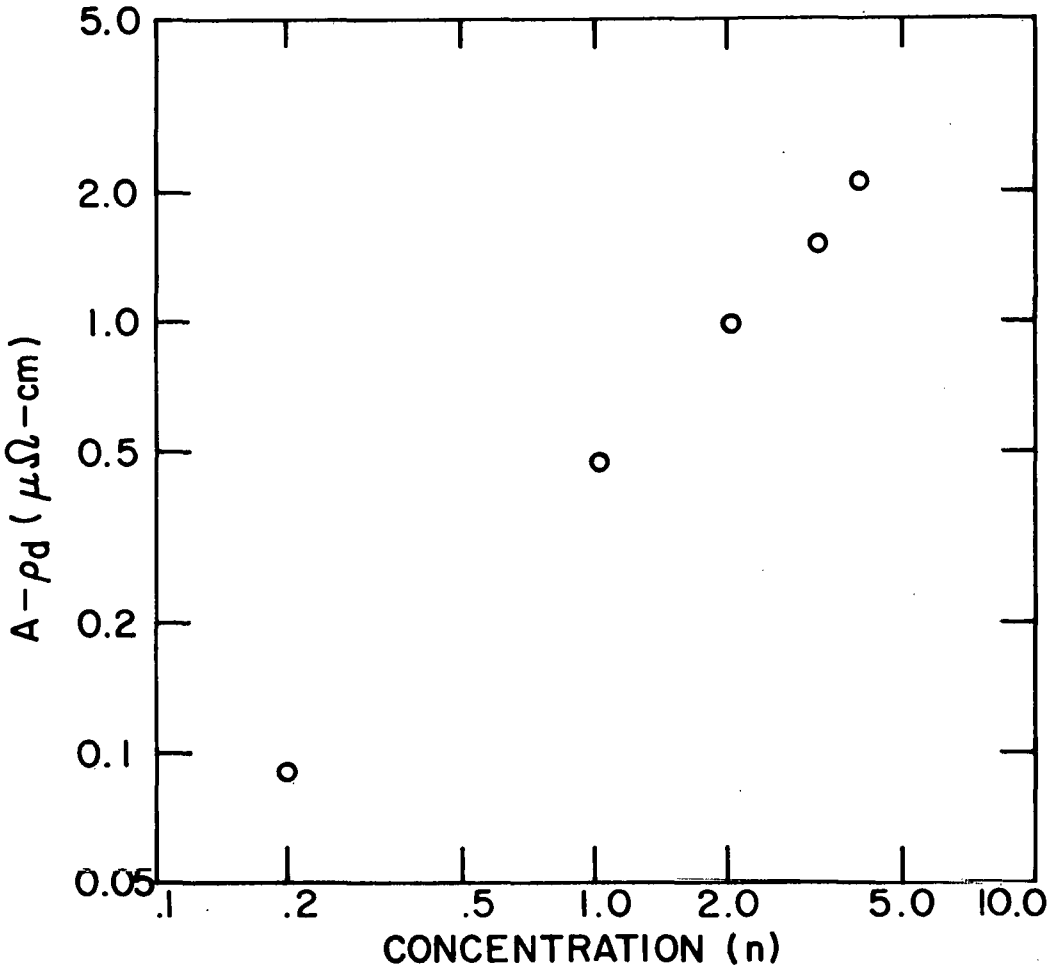

Figure 21. The temperature independent cerium potential scattering, A - ρ_d.

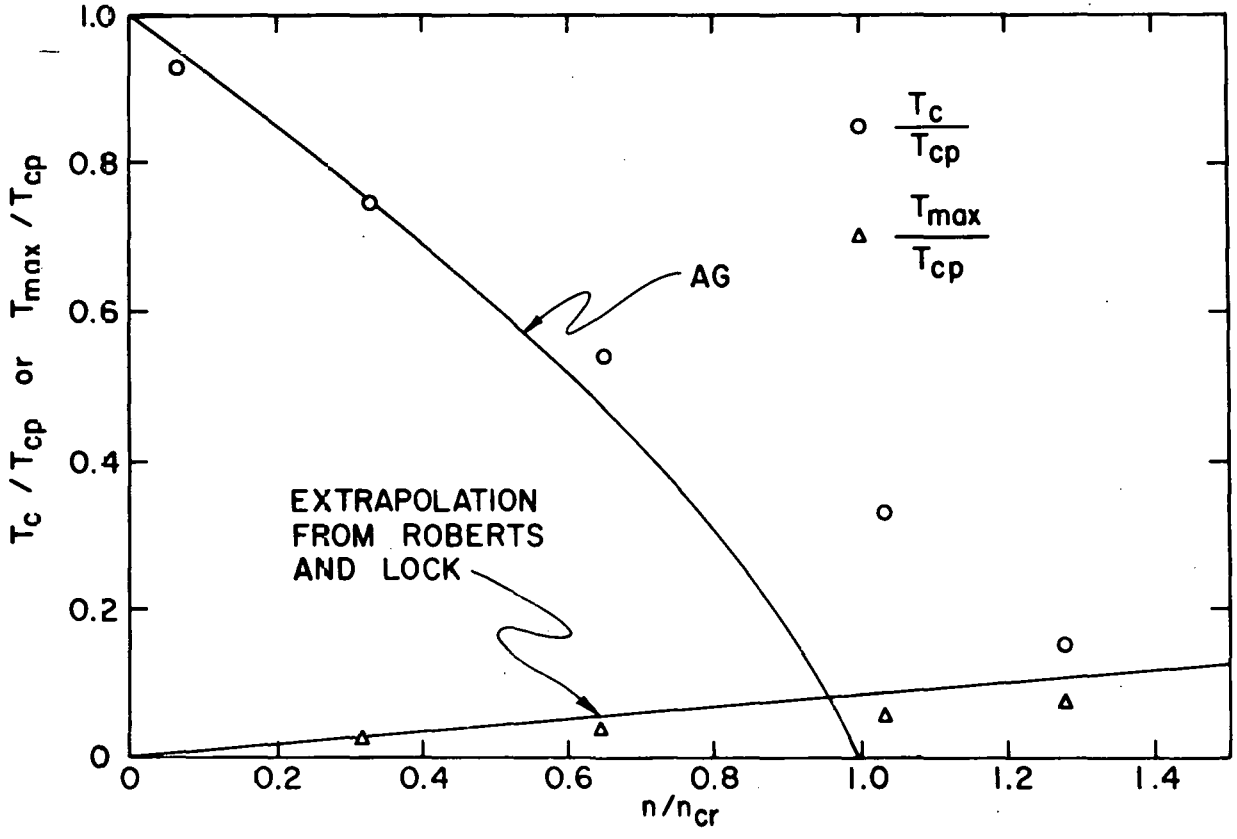

Figure 22. Deviations of the reduced critical temperature, T_c/T_{cp} from AG theory. The extrapolation of the upper specific heat anomaly measured by Roberts and Lock (57) shows reasonable agreement with the maximum in the normal state resistivity extrapolated to H = 0.

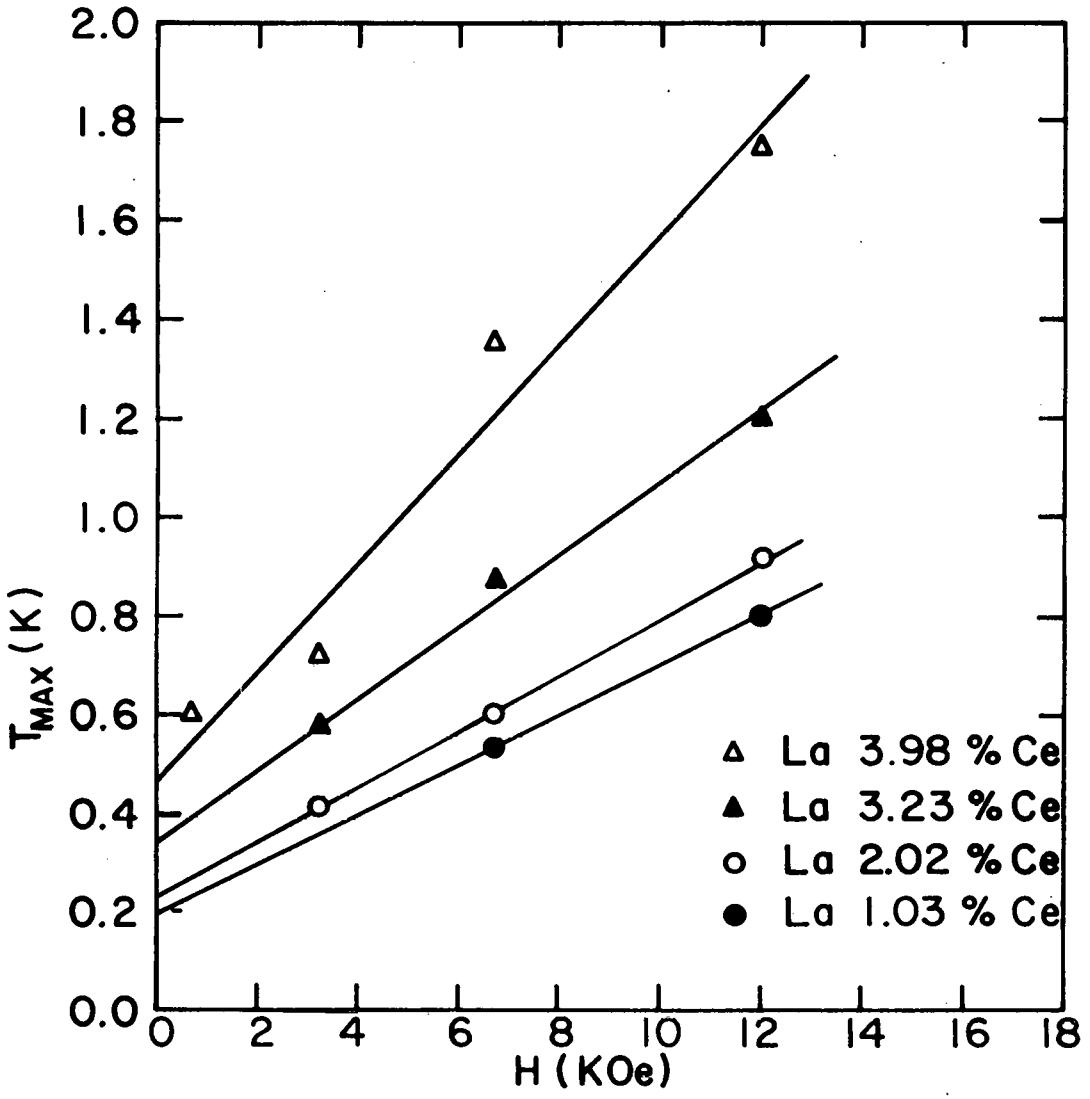

Figure 23. The temperature of the resistivity maximum, T_{max}, as a function of the applied field, H.

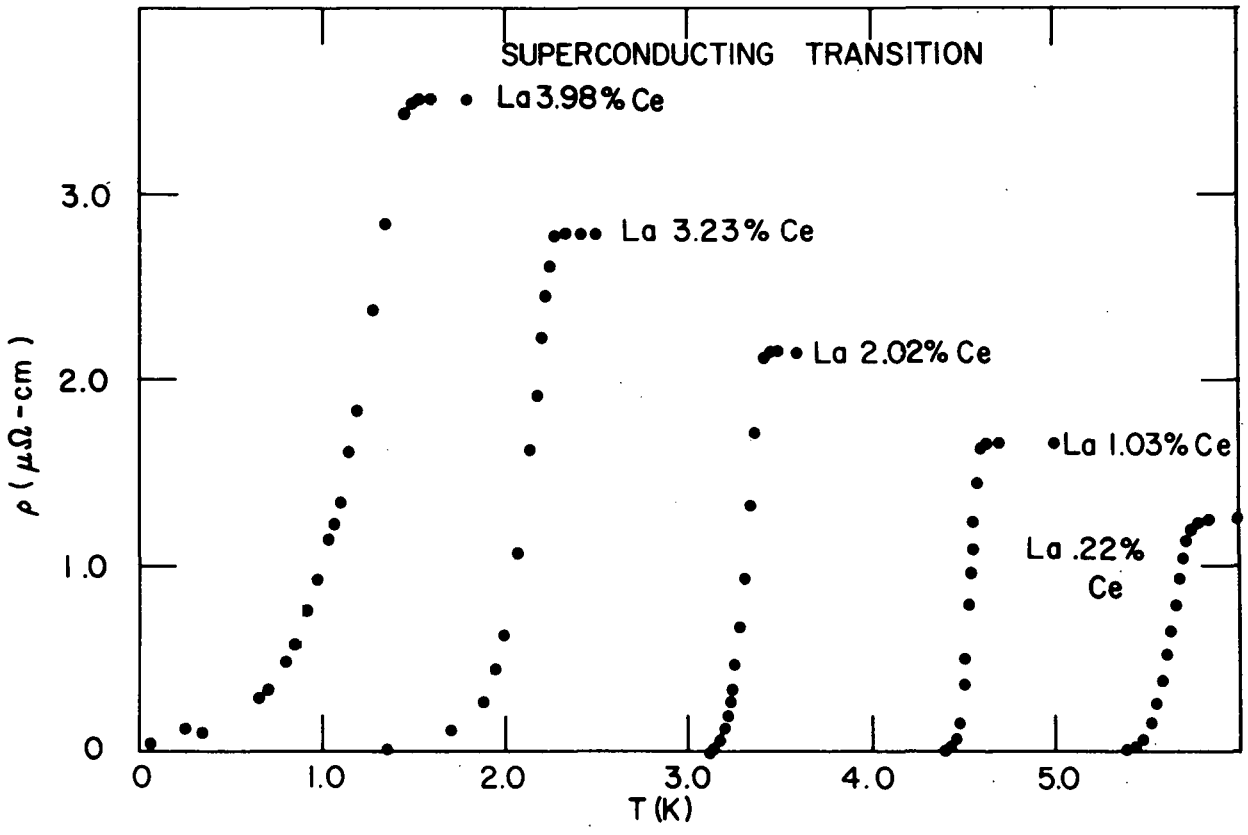

Figure 24. The zero field superconducting transitions for the five samples.

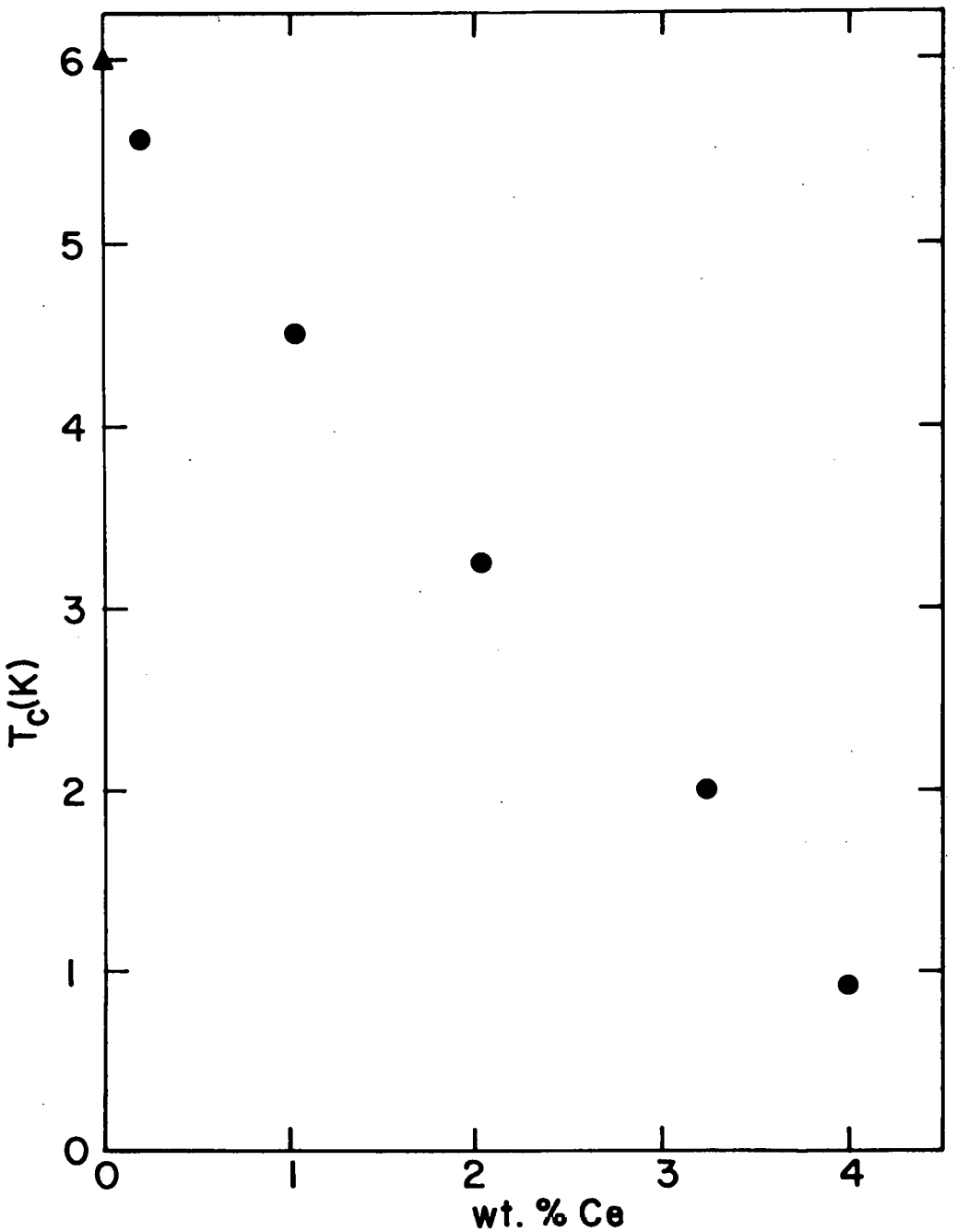

Figure 25. The depression in T_c for increasing cerium concentration. T_c for pure La is taken from Finnemore *et al.* (59).

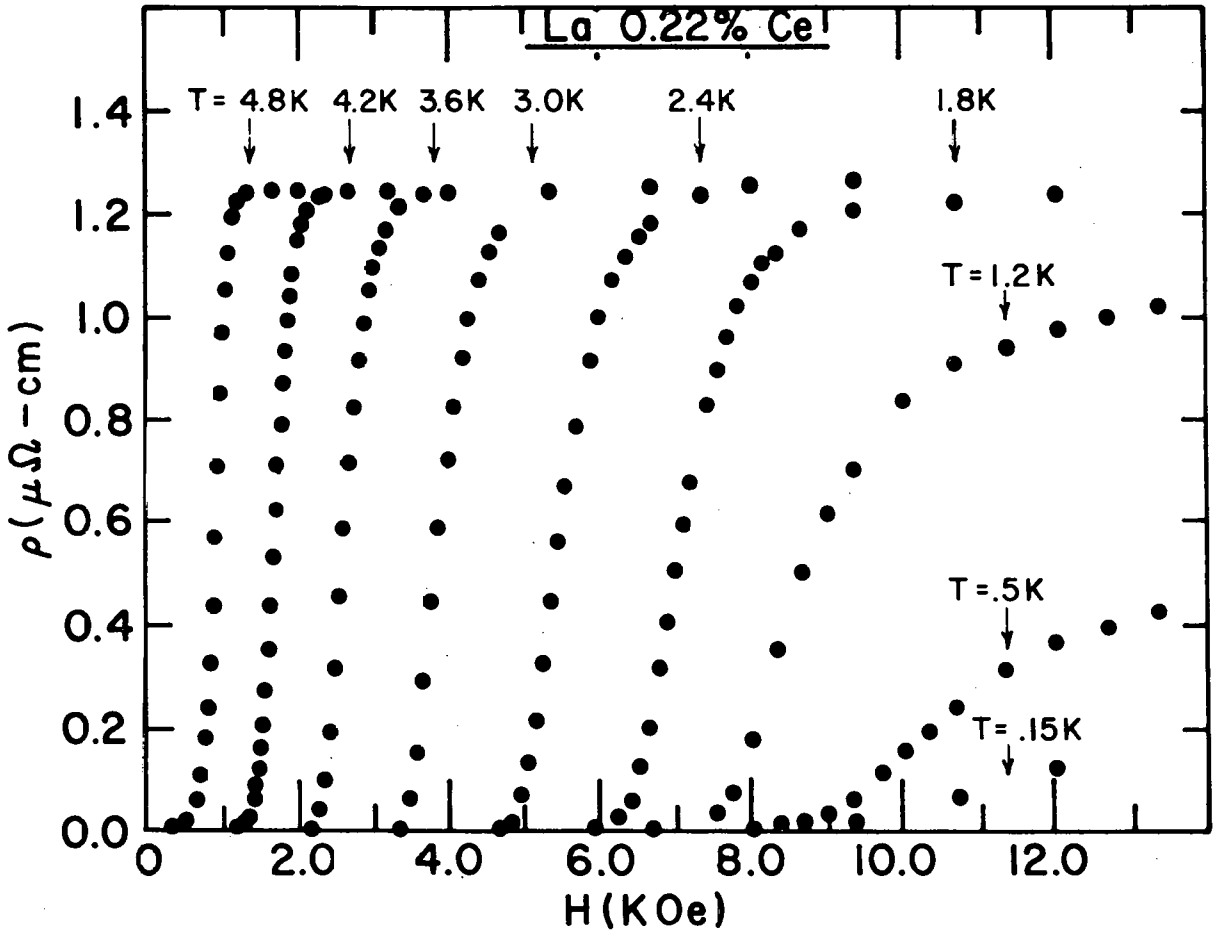

Figure 26. Superconducting transitions for La 0.22 % Ce.

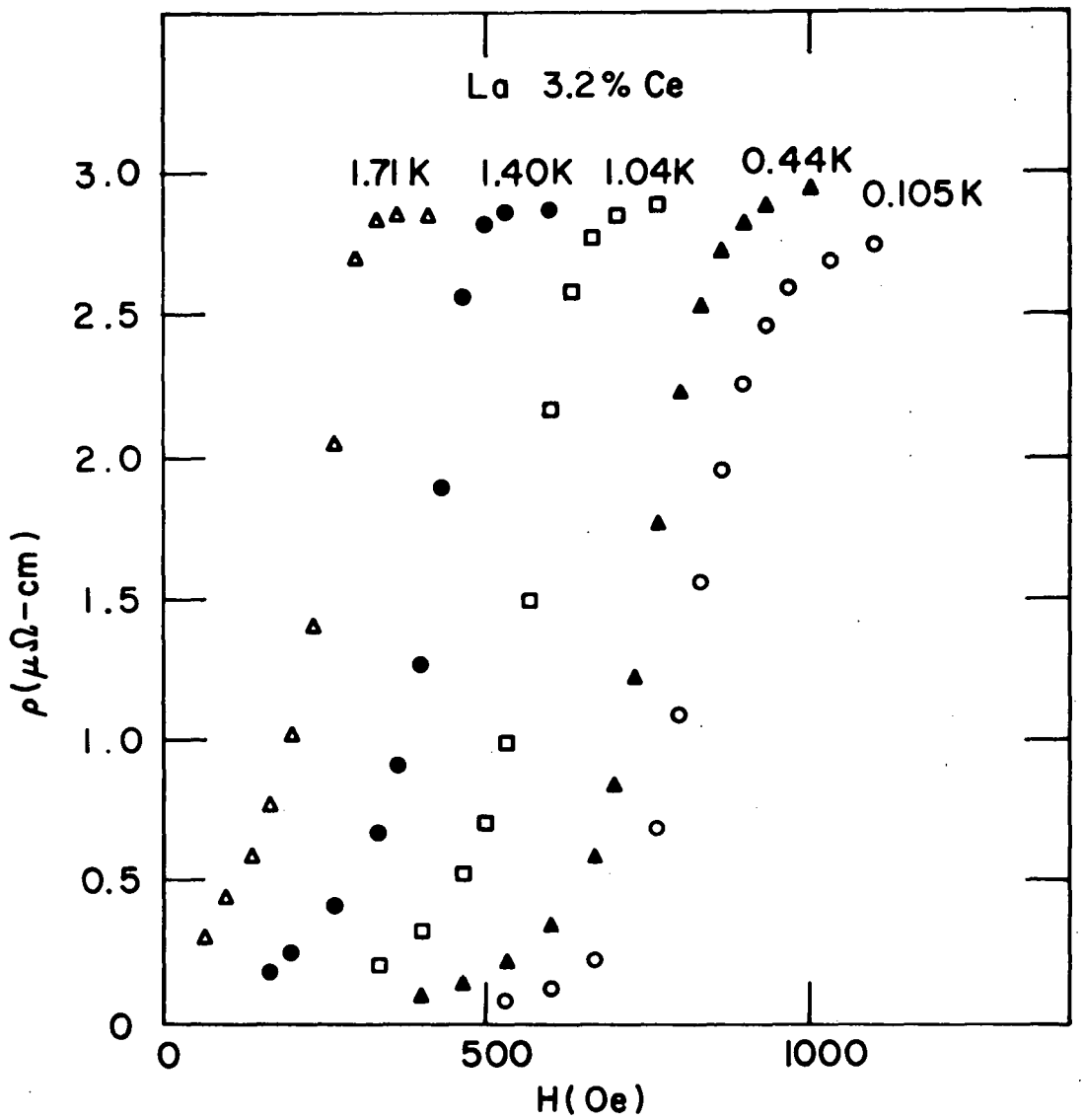

Figure 27. Superconducting transitions for La 3.23 % Ce.

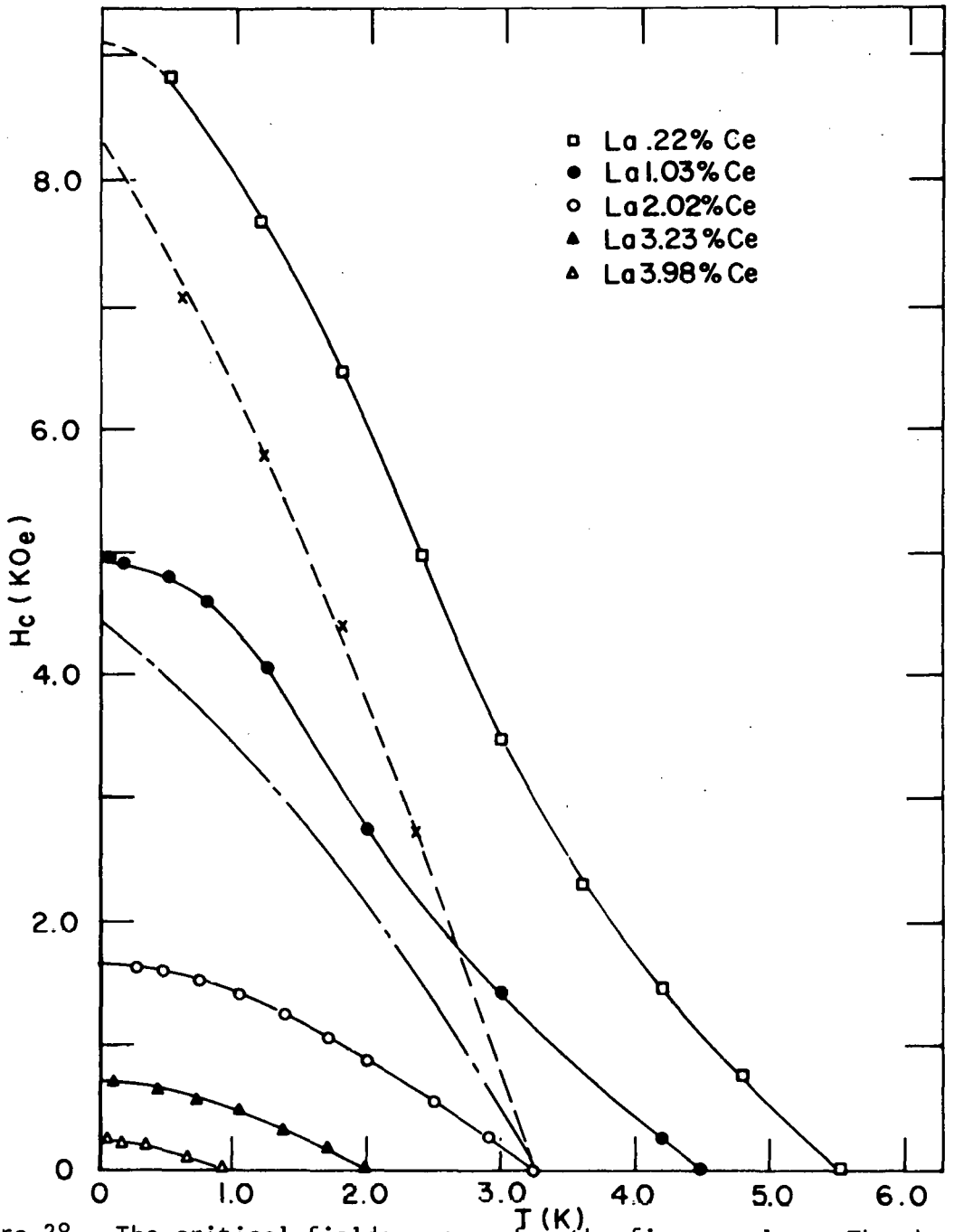

Figure 28. The critical fields curves for the five samples. The dot line represents the multiple pair breaking for the normal mean free path. The dot-dash line represents the multiple pair breaking theory corrected for mean free path.

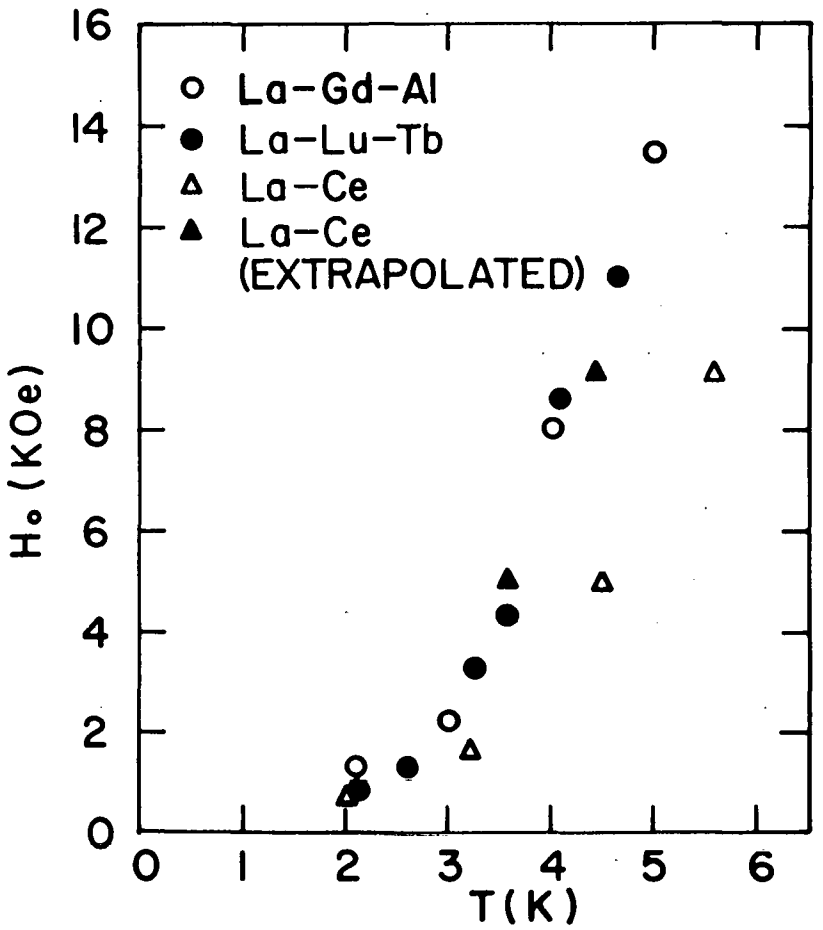

Figure 29. H_o versus T for various rare earth impurities in La which show the same exchange field enhancement effect independent of the sign of J. The extrapolated points for the La-Ce alloys correspond to the lower T_c values of the d-hcp extrapolation of critical field curves.

APPENDIX A

The following table gives the results of the chemical analysis which was used to check the cerium concentration of each alloy. The results are in weight percent not atomic percent. For these alloys this represents a difference ranging from 0.01 to 0.03% for the .2 and the 3.98% samples respectively. These values as given here were used throughout the analysis.

Table 7. Percent Ce determined by chemical analysis

Nominal percent Ce	Run 1	Run 2	Run 3	Run 4	Run 5	Run 6	Average wt. % Ce
.2	0.22	0.22	0.21	0.22	0.23		0.22
1.0	1.065	1.023	1.028	1.019			1.03
2.0	2.037	2.001	2.009	2.020			2.02
3.2	3.230	3.234	3.217	3.228			3.23
3.5	3.984	3.975	3.981	3.987	3.989	3.984	3.98

APPENDIX B

Table 8. AC calibration data for Gr 665

T,(K)	R,(ohms)	T,(K)	R,(ohms)
0.0594	93300	0.1914	2764
0.0692	58300	0.1979	2564
0.0696	57300	0.2115	2220
0.0748	44200	0.2268	1924
0.0776	38300	0.2270	1918
0.0780	37600	0.2384	1735
0.0785	37100	0.2602	1470
0.0822	31300	0.2759	1308
0.0822	31200	0.2902	1199
0.0853	26800	0.3099	1060
0.0855	26300	0.3196	1014
0.0897	22500	0.3510	867
0.0899	22300	0.3607	819.9
0.0948	18800	0.3939	720.8
0.0997	15900	0.4521	586.0
0.0998	15800	0.5074	497.4
0.1001	15700	0.5897	407.2
0.1077	12450	0.7034	327.8
0.1155	10100	0.8545	263.2
0.1157	10060		
0.1229	8450		
0.1230	8430		
0.1345	6580		
0.1346	6570		
0.1459	5307		
0.1562	4464		
0.1694	3667		
0.1965	3660		

Table 9. AC calibration data for Speer carbon resistor #8

T,(K)	R,(ohms)
0.0618	29400
0.0619	29200
0.0617	28600
0.0660	25430
0.0699	23270
0.0700	22940
0.0739	21010
0.0788	18460
0.0840	16620
0.0841	16380
0.0905	14400
0.0972	12740
0.1041	11240
0.1143	9593
0.1257	8203
0.1376	7058
0.1518	6044
0.1739	4933
0.1987	4070
0.1990	4064
0.2305	3329
0.2570	2889
0.2979	2413
0.3378	2086
0.3851	1807
0.4353	1591
0.4855	1431
0.5607	1252
0.6259	1138

Table 10. Resistivity ratios

Sample (wt. % Ce)	ρ_{295K} ($\mu\Omega$ - cm)	$\rho_{4.2K}$ ($\mu\Omega$ - cm)	$R_{4.2K}$ ($\mu\Omega$)	$H_{4.2K}$ (Oe)	$\frac{\rho_{295K}}{\rho_{4.2K}}$
.22	61.290	1.253	220	8040	48.91
1.03	62.453	1.667	428	3200	37.46
		1.674		6700	37.31
2.02	61.341	2.141	773	0	28.65
		2.142		3200	28.64
		2.141		6700	28.65
3.23	61.881	2.721	843	0	22.74
		2.723		3200	22.73
		2.729		6700	22.68
3.98	62.440	3.382	538	0	18.46
		3.382		3200	18.46
		3.382		6700	18.46

Table 11. Critical field data

T,(K)	H_{c2},(Oe)
La .22 wt. % Ce	
0.500	8820
1.200	7660
1.808	6450
2.40	4960
3.00	3480
3.605	2300
4.21	1470
4.802	764
La 1.03 wt. % Ce	
0.071	4960
0.178	4910
0.500	4800
0.800	4610
1.250	4070
1.995	2810
3.00	1440
4.20	250
La 2.02 wt. % Ce	
0.28	1628
0.44	1600
0.75	1527
1.041	1430
1.38	1256
1.71	1070
2.003	880
2.495	552
La 2.02 wt. % Ce	
2.90	260
La 2.23 wt. % Ce	
0.11	720
0.44	653
0.74	570
1.04	482
1.38	318
1.71	168
La 3.98 wt. % Ce	
0.060	250
0.170	216
0.350	189
0.658	100

Table 12. Superconducting transition data

T,(K)	ρ,(μΩ - cm)	T,(K)	ρ,(μΩ - cm)
La .22 wt. % Ce		La. 1.03 wt. % Ce	
5.393	0.0079	4.560	1.229
5.438	0.026	4.576	1.446
5.482	0.078	4.602	1.632
5.519	0.157	4.634	1.658
5.583	0.392	4.703	1.658
5.610	0.522	5.008	1.656
5.632	0.653		
5.655	0.7835	La 2.02 wt. % Ce	
5.680	0.9336	3.144	0.013
5.699	1.045	3.162	0.040
5.719	1.133	3.177	0.066
5.738	1.188	3.201	0.132
5.778	1.238	3.218	0.199
5.841	1.250	3.234	0.265
5.999	1.252	3.241	0.331
		3.260	0.463
La 1.03 wt. % Ce		3.283	0.662
4.411	0.0068	3.309	0.927
4.438	0.0272	3.340	1.324
4.460	0.068	3.373	1.721
4.476	0.143	3.417	2.118
4.504	0.363	3.450	2.149
4.516	0.499	3.500	2.147
4.525	0.635	3.606	2.143
4.535	0.789		
4.545	0.952	La 3.23 wt. % Ce	
4.552	1.088	1.377	0.006
		1.712	0.119

Table 12. (Continued)

T,(K)	ρ,(μΩ - cm)	T,(K)	ρ,(μΩ - cm)
La 3.23 wt. % Ce		La 3.98 wt. % Ce	
1.885	0.273	1.097	1.337
1.950	0.442	1.154	1.615
2.000	0.631	1.197	1.827
2.079	1.067	1.285	2.368
2.123	1.408	1.356	2.843
2.150	1.626	1.449	3.493
2.180	1.922	1.802	3.501
2.210	2.223		
2.230	2.446		
2.250	2.619		
2.281	2.769		
2.340	2.790		
2.421	2.785		
2.498	2.781		
La 3.98 wt. % Ce			
0.066	0.044		
0.253	0.124		
0.350	0.102		
0.658	0.285		
0.703	0.336		
0.802	0.482		
0.852	0.577		
0.918	0.760		
0.977	0.921		
1.043	1.140		
1.070	1.228		

APPENDIX C

Table 13. Sample 1 La .22 wt. % Ce

T (K)	ρ ($\mu\Omega$ - cm)	$\rho-\rho_o$ ($\mu\Omega$ - cm)	T (K)	ρ ($\mu\Omega$ - cm)	$\rho-\rho_o$ ($\mu\Omega$ - cm)
	H = 0			H = 6700 Oe	
5.999	1.252	0.221	2.599	1.240	0.368
6.389	1.262	0.202	2.803	1.256	0.379
6.794	1.273	0.181	3.006	1.256	0.373
7.090	1.284	0.167	3.202	1.256	0.367
7.400	1.297	0.152	3.402	1.254	0.358
7.714	1.310	0.136	3.634	1.252	0.348
8.105	1.332	0.119	3.672	1.252	0.347
8.598	1.365	0.099	4.215	1.250	0.322
9.317	1.422	0.072	4.221	1.249	0.321
9.995	1.488	0.051	4.497	1.250	0.309
10.987	1.604	0.027	4.801	1.251	0.294
11.977	1.747	0.012	4.826	1.250	0.292
13.018	1.920	0.001	5.200	1.252	0.273
14.170	2.144	-0.001	5.576	1.257	0.254
15.020	2.326	-0.001	5.994	1.263	0.232
16.203	2.602	-0.001			
17.413	2.921	0.008		H = 12000 Oe	
18.927	3.339	-0.001	2.402	1.266	0.399
19.935	3.643	-0.006			
	H = 3200 (3350) Oe				
3.608	1.210	0.307			
4.210	1.243	0.315			
5.203	1.246	0.266			
5.582	1.250	0.247			
5.994	1.256	0.225			

Table 14. Sample 2 La 1.03 wt. % Ce

T (K)	ρ ($\mu\Omega$ - cm)	$\rho-\rho_o$ ($\mu\Omega$ - cm)	T (K)	ρ ($\mu\Omega$ - cm)	$\rho-\rho_o$ ($\mu\Omega$ - cm)
	H = 0			H = 6700 0e	
4.634	1.658	0.366	0.172	1.748	0.532
5.297	1.654	0.295	0.178	1.750	0.534
5.621	1.655	0.275	0.193	1.760	0.544
5.993	1.657	0.252	0.198	1.764	0.548
6.535	1.666	0.220	0.214	1.770	0.554
7.010	1.678	0.193	0.226	1.766	0.550
7.497	1.697	0.168	0.234	1.789	0.565
7.795	1.710	0.153	0.245	1.786	0.570
8.477	1.751	0.123	0.268	1.794	0.578
9.225	1.807	0.092	0.272	1.791	0.575
10.455	1.931	0.054	0.288	1.804	0.588
11.995	2.140	0.024	0.296	1.806	0.590
14.035	2.502	0.004	0.303	1.809	0.593
16.015	2.942	0.001	0.320	1.809	0.593
18.105	3.481	-0.008	0.331	1.814	0.600
			0.366	1.822	0.608
	H = 6700 0e		0.369	1.818	0.602
0.081	1.659	0.443	0.388	1.825	0.609
0.086	1.664	0.448	0.409	1.832	0.616
0.094	1.673	0.457	0.494	1.840	0.623
0.108	1.682	0.466	0.500	1.840	0.623
0.124	1.698	0.482	0.500	1.836	0.619
0.138	1.714	0.498	0.502	1.838	0.621
0.152	1.723	0.507	0.511	1.840	0.623
0.155	1.733	0.517	0.579	1.836	0.619
0.169	1.747	0.531	0.579	1.838	0.621
0.170	1.736	0.520	0.585	1.839	0.622

Table 14. (Continued)

T (K)	ρ ($\mu\Omega$ - cm)	$\rho-\rho_o$ ($\mu\Omega$ - cm)	T (K)	ρ ($\mu\Omega$ - cm)	$\rho-\rho_o$ ($\mu\Omega$ - cm)
	H = 6700 0e			H = 6700 0e	
0.685	1.836	0.619	4.202	1.675	0.374
0.685	1.834	0.617	4.225	1.674	0.372
0.690	1,835	0.618	4.435	1.671	0.359
0.800	1.828	0.610	5.001	1.666	0.324
0.800	1.831	0.613	5.283	1.665	0.307
0.886	1.822	0.603	5.480	1.665	0.295
0.956	1.816	0.597	5.995	1.668	0.263
1.042	1.810	0.590	6.527	1.676	0.231
1.139	1.802	0.581	6.997	1.688	0.204
1.249	1.794	0.572	7.780	1.719	0.163
1.380	1.785	0.562	8.475	1.759	0.131
1.402	1.783	0.560	9.227	1.814	0.099
1.606	1.769	0.543			
1.800	1.758	0.529		H = 12000 0e	
1.995	1.748	0.516	0.082	1.621	0.405
2.002	1.747	0.515	0.492	1.796	0.579
2.201	1.737	0.501	0.967	1.803	0.584
2.404	1.727	0.487	1.405	1.780	0.557
2.600	1.719	0.474	2.002	1.750	0.518
2.801	1.712	0.462	4.234	1.681	0.379
2.995	1.705	0.449			
3.191	1.699	0.437			
3.396	1.693	0.424			
3.598	1.687	0.411			
3.803	1.682	0.398			
3.996	1.678	0.386			

Table 15. Sample 3 La 2.02 wt. % Ce

T (K)	ρ ($\mu\Omega$ - cm)	$\rho-\rho_o$ ($\mu\Omega$ - cm)	T (K)	ρ ($\mu\Omega$ - cm)	$\rho-\rho_o$ ($\mu\Omega$ - cm)
	H = 0			H = 0	
1.468	2.277	0.538	9.015	2.226	0.072
1.641	2.259	0.518	10.015	2.306	0.040
1.710	2.261	0.519	12.05	2.550	0.008
1.727	2.261	0.519	13.96	2.859	-0.001
2.122	2.229	0.481	16.15	3.297	0.000
2.575	2.205	0.448	18.10	3.755	0.000
3.426	2.142	0.362			
3.484	2.147	0.365		H = 3200 Oe	
3.574	2.145	0.360	0.107	2.290	0.558
3.670	2.142	0.354	0.114	2.278	0.546
3.760	2.141	0.350	0.129	2.311	0.579
3.840	2.138	0.344	0.137	2.317	0.584
3.930	2.133	0.336	0.157	2.328	0.592
4.068	2.149	0.347	0.162	2.336	0.604
4.206	2.146	0.338	0.171	2.340	0.608
4.206	2.140	0.332	0.191	2.353	0.621
4.260	2.140	0.330	0.214	2.363	0.631
4.386	2.137	0.322	0.220	2.362	0.630
4.755	2.130	0.298	0.236	2.379	0.647
5.073	2.127	0.279	0.254	2.375	0.643
5.496	2.123	0.253	0.258	2.385	0.653
5.988	2.122	0.222	0.287	2.385	0.653
6.494	2.126	0.192	0.292	2.389	0.657
6.992	2.135	0.165	0.324	2.394	0.662
7.520	2.149	0.137	0.356	2.389	0.657
8.000	2.166	0.112	0.387	2.402	0.670

Table 15. (Continued)

T (K)	ρ ($\mu\Omega$ - cm)	$\rho-\rho_o$ ($\mu\Omega$ - cm)	T (K)	ρ ($\mu\Omega$ - cm)	$\rho-\rho_o$ ($\mu\Omega$ - cm)
	H = 3200 Oe			H = 6700 Oe	
0.439	2.400	0.668	2.490	2.185	0.430
0.440	2.391	0.655	3.428	2.164	0.388
0.443	2.398	0.666	4.209	2.135	0.327
0.452	2.398	0.666			
0.493	2.391	0.658		H = 12000 Oe	
0.517	2.389	0.657	0.114	1.998	0.266
0.603	2.370	0.637	0.356	2.164	0.432
0.646	2.376	0.643	0.832	2.253	0.519
0.695	2.362	0.629	1.000	2.253	0.518
0.771	2.353	0.619	1.668	2.217	0.476
0.809	2.344	0.610	3.420	2.158	0.382
0.851	2.338	0.604	4.214	2.137	0.329
0.992	2.321	0.586			
1.041	2.318	0.583			
1.182	2.309	0.573			
1.378	2.292	0.554			
1.709	2.258	0.516			
2.004	2.236	0.490			
2.488	2.192	0.437			
2.896	2.171	0.406			
	H = 6700 Oe				
0.107	2.099	0.367			
0.437	2.296	0.564			
0.821	2.291	0.557			
1.375	2.260	0.522			
2.000	2.222	0.476			

Table 16. Sample 4 La 3.23 wt. % Ce

T (K)	ρ ($\mu\Omega$ - cm)	$\rho-\rho_o$ ($\mu\Omega$ - cm)	T (K)	ρ ($\mu\Omega$ - cm)	$\rho-\rho_o$ ($\mu\Omega$ - cm)
	H = 0			H = 3200 Oe	
2.281	2.769	0.504	0.127	2.712	0.467
2.340	2.790	0.524	0.156	2.757	0.512
2.421	2.785	0.517	0.175	2.779	0.534
2.498	2.781	0.511	0.204	2.809	0.564
2.900	2.761	0.481	0.219	2.824	0.579
3.205	2.749	0.460	0.236	2.838	0.593
3.611	2.729	0.427	0.254	2.853	0.608
4.105	2.720	0.399	0.284	2.875	0.630
4.207	2.728	0.403	0.315	2.890	0.645
4.383	2.721	0.388	0.324	2.890	0.645
4.750	2.709	0.358	0.382	2.913	0.668
5.077	2.702	0.338	0.389	2.910	0.665
5.495	2.695	0.304	0.436	2.917	0.672
5.990	2.689	0.266	0.439	2.920	0.675
6.494	2.690	0.232	0.450	2.920	0.674
7.007	2.696	0.198	0.517	2.923	0.677
7.508	2.708	0.167	0.646	2.920	0.674
8.013	2.727	0.140	0.773	2.913	0.666
8.995	2.784	0.095	0.810	2.908	0.661
10.020	2.870	0.059	0.890	2.902	0.655
12.015	3.111	0.015	0.989	2.905	0.657
13.97	3.439	-0.001	1.041	2.893	0.645
16.00	3.869	0.002	1.182	2.883	0.633
18.25	4.432	0.006	1.378	2.871	0.619
			1.709	2.843	0.587
	H = 3200 Oe		2.004	2.825	0.565
0.107	2.668	0.423	2.488	2.792	0.522

Table 16. (Continued)

T (K)	ρ ($\mu\Omega$ - cm)	$\rho - \rho_o$ ($\mu\Omega$ - cm)
	H = 3200 Oe	
2.896	2.773	0.493
3.205	2.763	0.474
4.109	2.723	0.402
	H = 6700 Oe	
0.108	2.505	0.260
0.437	2.804	0.559
0.793	2.860	0.613
0.795	2.868	0.621
1.375	2.849	0.598
2.000	2.819	0.559
2.490	2.790	0.520
4.207	2.729	0.404
	H = 1200 Oe	
0.109	2.431	0.186
0.443	2.715	0.469
0.799	2.816	0.569
1.375	2.827	0.576
2.000	2.812	0.552
2.492	2.791	0.521
4.213	2.729	0.404

Table 17. Sample 5 La 3.98 wt. % Ce

T (K)	ρ ($\mu\Omega$ - cm)	$\rho-\rho_o$ ($\mu\Omega$ - cm)	T (K)	ρ ($\mu\Omega$ - cm)	$\rho-\rho_o$ ($\mu\Omega$ - cm)
	H = 0			H = 0	
1.487	3.484	0.633	6.197	3.330	0.290
1.535	3.509	0.657	6.392	3.329	0.274
1.609	3.509	0.657	6.796	3.330	0.244
1.802	3.501	0.646	7.100	3.333	0.222
2.002	3.493	0.634	7.405	3.338	0.200
2.195	3.484	0.622	7.705	3.346	0.181
2.402	3.473	0.607	8.110	3.361	0.157
2.600	3.463	0.592	8.593	3.385	0.130
2.803	3.452	0.576	9.320	3.431	0.094
3.002	3.440	0.558	9.987	3.489	0.069
3.197	3.430	0.543	10.996	3.597	0.037
3.391	3.421	0.527	11.983	3.731	0.018
3.584	3.411	0.510	13.018	3.897	0.006
3.797	3.401	0.492	14.150	4.106	-0.001
3.993	3.392	0.476	15.020	4.288	-0.001
4.197	3.382	0.457	16.192	4.556	0.001
4.264	3.378	0.450	17.430	4.864	-0.001
4.264	3.380	0.452	18.905	5.270	0.000
4.395	3.374	0.440	19.950	5.570	-0.012
4.609	3.366	0.422			
4.816	3.359	0.404		H = 670 Oe	
5.002	3.353	0.388	0.060	3.05	0.21
5.202	3.348	0.372	0.0617	3.06	0.22
5.398	3.342	0.354	0.0630	3.082	0.239
5.584	3.339	0.340	0.0647	3.094	0.251
5.800	3.335	0.322	0.0661	3.100	0.257
5.999	3.332	0.306	0.0675	3.107	0.264

Table 17. (Continued)

T (K)	ρ ($\mu\Omega$ - cm)	$\rho-\rho_o$ ($\mu\Omega$ - cm)	T (K)	ρ ($\mu\Omega$ - cm)	$\rho-\rho_o$ ($\mu\Omega$ - cm)
	H = 670 Oe			H = 670 Oe	
0.0722	3.12	0.28	0.497	3.566	0.702
0.0769	3.14	0.30	0.499	3.552	0.708
0.0785	3.155	0.312	0.551	3.556	0.712
0.0847	3.176	0.333	0.600	3.556	0.712
0.0944	3.20	0.36	0.660	3.554	0.710
0.0955	3.209	0.366	0.729	3.552	0.707
0.106	3.243	0.400	0.800	3.548	0.703
0.1144	3.263	0.420	0.900	3.542	0.696
0.130	3.297	0.454	1.020	3.536	0.690
0.143	3.321	0.478	1.200	3.527	0.679
0.158	3.347	0.504	1.400	3.518	0.668
0.167	3.360	0.517	1.497	3.566	0.702
0.169	3.368	0.525	1.800	3.501	0.646
0.179	3.378	0.535	2.400	3.473	0.607
0.195	3.401	0.558			
0.217	3.427	0.584		H = 3200 Oe	
0.245	3.455	0.612	0.085	3.08	0.24
0.253	3.463	0.620	0.1145	3.16	0.32
0.258	3.468	0.625	0.140	3.22	0.38
0.294	3.490	0.647	0.149	3.243	0.400
0.336	3.513	0.670	0.160	3.25	0.41
0.348	3.517	0.674	0.198	3.334	0.491
0.360	3.522	0.679	0.207	3.32	0.48
0.398	3.536	0.693	0.220	3.362	0.519
0.444	3.546	0.702	0.253	3.387	0.544
0.483	3.551	0.707	0.343	3.455	0.612

Table 17. (Continued)

T (K)	ρ ($\mu\Omega$ - cm)	$\rho-\rho_o$ ($\mu\Omega$ - cm)	T (K)	ρ ($\mu\Omega$ - cm)	$\rho-\rho_o$ ($\mu\Omega$ - cm)
H = 3200 Oe			H = 12000 Oe		
0.360	3.467	0.624	0.0914	2.83	-0.01
0.498	3.511	0.667	0.152	2.95	0.11
0.773	3.3528	0.683	0.215	3.05	0.21
0.893	3.526	0.680	0.254	3.08	0.24
1.200	3.518	0.670	0.499	3.29	0.45
1.802	3.498	0.643	0.884	3.41	0.565
2.402	3.471	0.605	1.201	3.442	0.594
4.210	3.382	0.456	1.807	3.464	0.609
			2.402	3.45	0.58
H = 6700 Oe			4.220	3.375	0.449
0.0864	2.96	0.12			
0.150	3.08	0.124			
0.254	3.23	0.39			
0.498	3.400	0.556			
0.800	3.46	0.62			
0.893	3.48	0.64			
1.199	3.487	0.639			
1.806	3.487	0.632			
2.403	3.466	0.600			
2.600	3.455	0.584			
2.812	3.446	0.570			
3.006	3.435	0.553			
3.202	3.427	0.539			
3.382	3.419	0.525			
4.214	3.382	0.456			

APPENDIX D

The resistivity of pure Ce was measured from 0.071 K to 295 K. The data are given in the following table, and $\rho-\rho_d$, the total resistivity minus the residual resistivity due to unwanted impurities is shown in Figure 30.

Table 18. Pure cerium

T (K)	ρ ($\mu\Omega$ - cm)	$\rho-\rho_d$ ($\mu\Omega$ - cm)	T (K)	ρ ($\mu\Omega$ - cm)	$\rho-\rho_d$ ($\mu\Omega$ - cm)
ρ_d = 2.9427 $\mu\Omega$ - cm			ρ_d = 2.9437 $\mu\Omega$ - cm		
0.071	2.9437	0.1	4.501	4.703	1.759
0.260	2.9437	0.0	4.800	5.010	2.066
0.315	2.9451	0.0014	5.088	5.319	2.375
0.383	2.9469	0.0032	5.404	5.678	2.734
0.469	2.9511	0.0074	5.700	6.027	3.083
0.559	2.9553	0.0116	6.002	6.395	3.451
0.700	2.9623	0.0186	6.306	6.758	3.814
0.804	2.969	0.025	6.984	7.544	4.600
0.992	2.983	0.039	8.025	8.689	5.745
1.165	2.999	0.055	9.000	9.701	6.757
1.209	3.004	0.060	10.025	10.658	7.714
1.590	3.055	0.111	11.55	11.949	9.005
1.997	3.132	0.188	13.00	12.971	10.027
2.402	3.246	0.302	14.44	13.601	10.657
2.752	3.383	0.439	16.06	14.064	11.120
3.004	3.504	0.560	18.08	14.683	11.739
3.240	3.644	0.700	19.95	15.309	12.365
3.506	3.821	0.877	31.±1	19.151	16.207
3.755	4.012	1.068	51.±1	25.457	22.513
4.000	4.228	1.284			
4.201	4.406	1.462			
4.292	4.500	1.556			
295.	74.891	71.947	(before cooling)		
295.	80.426	77.482	(after cooling)		

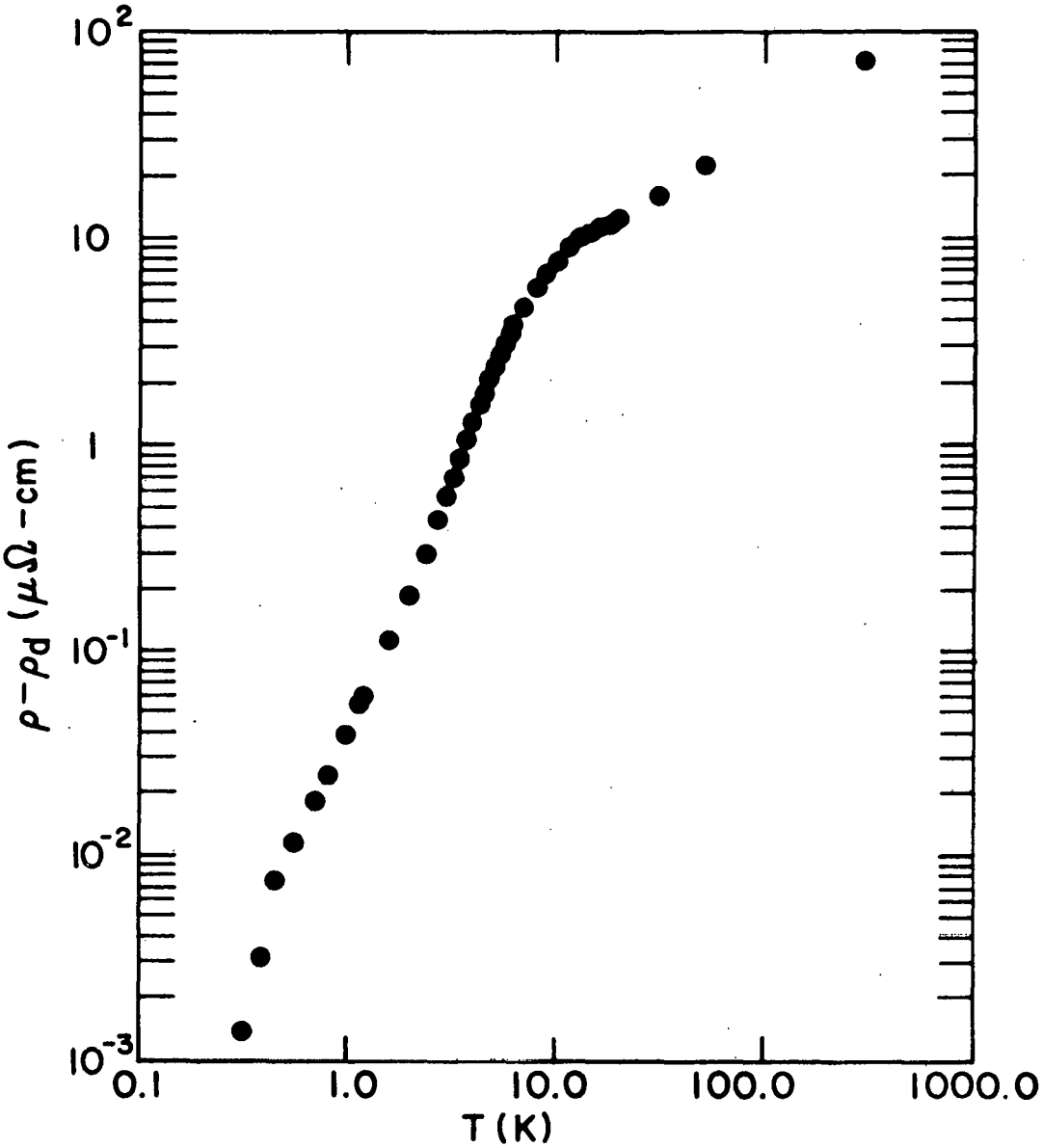

Figure 30. The intrinsic resistivity of pure cerium.